AEC
RESEARCH
and
DEVELOPMENT
REPORT

BNWL-100

29-

HIGH TEMPERATURE CORROSION OF CANDIDATE ATR STRUCTURAL MATERIALS

L. A. CHARLOT and R. E. WESTERMAN

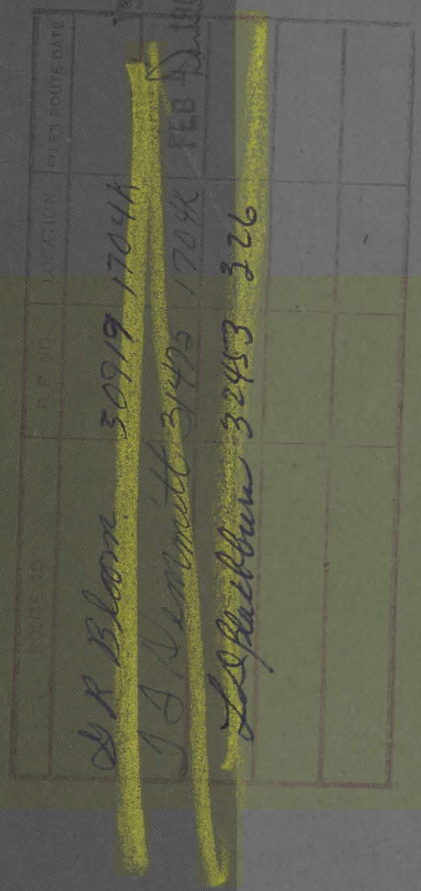

SEPTEMBER, 1965

BATTELLE-NORTHWEST
RICHLAND, WASHINGTON

PACIFIC NORTHWEST LABORATORY operated by BATTELLE MEMORIAL INSTITUTE

LEGAL NOTICE

PACIFIC NORTHWEST LABORATORY
RICHLAND, WASHINGTON
operated by
BATTELLE MEMORIAL INSTITUTE
for the
UNITED STATES ATOMIC ENERGY COMMISSION UNDER CONTRACT AT(45-1)-1830

PRINTED BY/FOR THE U. S. ATOMIC ENERGY COMMISSION

AEC-RLOO RICHLAND, WASH.

BNWL-100
UC-25, Metals, Ceramics
and Materials

HIGH TEMPERATURE CORROSION OF CANDIDATE ATR STRUCTURAL MATERIALS

By
L. A. Charlot and R. E. Westerman

Metallurgy Research Section
Reactor and Materials Technology Department

September, 1965

PACIFIC NORTHWEST LABORATORY
RICHLAND, WASHINGTON

TABLE OF CONTENTS

HIGH TEMPERATURE CORROSION OF CANDIDATE ATR STRUCTURAL MATERIALS

INTRODUCTION

Research data in support of the Advanced Test Reactor (ATR) program of compatibility between structural material and gas are presented.

Hastelloy X, Haynes Alloy 25, and Inconel 600 are being considered as structural materials in the ATR Gas Loop. Because of the high temperatures which will be attained in the test section and associated piping (over 2000 ^{o}F), the service will be extremely severe, and any degradation of the material which might occur must be taken into account in the initial design and subsequent operation of the loop. This report evaluates superalloys in various high temperature gaseous corrosive environments.

The structural materials in the ATR loop will be exposed to high temperature, high velocity helium gas containing trace contaminants. Under these conditions, three distinct degradation phenomena may be encountered.

- Chemical reaction with trace contaminants in the helium. Scaling reactions, subscale reactions, and solution effects are included.
- Evaporation of structural materials (vapor pressure effect).
- Erosion of structural materials by mechanical removal of metal or corrosion product by the high velocity helium.

Chemical Reaction

The chemical reaction of a structural material with its environment is true corrosion. Because the helium gas is inert, we need only consider chemical reactions between the structural materials and trace amounts of oxygen, nitrogen, hydrogen, water vapor, and carbon oxides. Aim helium purity is 1 vpm total contaminant.

Consider first the potentially most serious problem, that of oxidation. Nickel and cobalt, the base elements of the alloys under consideration, will theoretically form stable oxides at 2000 ^{o}F (1093 ^{o}C) if the

oxygen partial pressure becomes as high as 10^{-8} atm, or about 0.01 μ.[1] More reactive constituents, such as chromium, will oxidize at much lower oxygen pressures.[2] At 1 vpm total impurity level in helium gas at 300 psi, the contaminant partial pressure is 16 μ.* Then, oxidation is likely if oxygen constitutes even a small fraction of the total trace contaminant.

Ideally, conservation of structural integrity could be guaranteed (from a corrosion standpoint) by either one of two approaches:

- Limit the access of reactive impurities to the structural materials by only circulating ultrapure helium of inconsequential impurity content in a completely clean, leakfree system, or
- Utilize structural materials of such high oxidation resistance that relatively large partial pressures of contaminant can be tolerated more or less continuously.

Since neither case is completely attainable in actual practice, consideration must be given to both helium cleanliness and alloy corrosion resistance.

Evaporation

Evaporation rates of structural materials become a potentially important problem at temperatures in excess of 2000 °F. Rosenthal[3] has briefly discussed this problem and concludes that it is possible that evaporation of metals into a high velocity gas stream might approach the conditions which would prevail in a vacuum, even though the presence of a high pressure inert gas will retard evaporation.

Erosion

Erosion (and evaporation, for that matter) of structural materials cannot be evaluated in the same manner as chemical reaction. For meaningful results on erosion and evaporation effects, a high temperature, high velocity gas facility has been built (Dynamic Materials Testing Apparatus, DMTA). However, even with good data concerning erosion, evaporation, and chemical reaction from the DMTA, careful monitoring of both environment and metal test samples must be employed during the actual operation of the ATR loop in order to ascertain structural damage by any of these mechanisms.

---

* 1 micron (μ) is equal to 0.001 Torr.

SUMMARY

The investigations were concerned primarily with the behavior of Hastelloy X-280, a nickel-base alloy, and Haynes Alloy 25, a cobalt-base alloy, in static atmospheres of oxygen, methane, carbon monoxide, carbon dioxide, nitrogen, flowing helium, and water vapor at temperatures of 2048 and 2192 ^{o}F (1120 and 1200 ^{o}C). Evaporation rates of the alloys, and corrosion of weldments in contaminated helium were also studied.

Kinetic analyses of the gas-metal reactions were based on continuous weight change determinations. Metallography was employed to evaluate the microstructure of the corroded samples.

1) At 2192 ^{o}F, Hastelloy X-280 and Inconel 600 demonstrate an oxidation resistance which would permit their use in oxidizing atmospheres for short periods of time, e.g., a few hours in air, with only moderate attack. Haynes Alloy 25 cannot be exposed to atmospheres containing a higher oxygen partial pressure than about 0.3 Torr at 2192 ^{o}F, even for short times, without risk of catastrophic attack.

2) For longtime service at 2192 ^{o}F, two potentially dangerous modes of attack must be considered: oxidation and evaporation. The relative magnitude of each effect depends on the oxidant pressure. If the oxidant pressure is so low that oxidation of the sample surface does not take place, the alloy will tend to evaporate. Haynes Alloy 25, Hastelloy X-280, and Inconel 600 evaporate at similar rates at 2192 ^{o}F under vacuum conditions (pressures $\sim 10^{-4}$ Torr). Oxygen pressures less than the dissociation pressure of chromium or nickel are not required in a vacuum system for evaporation to take place presumably because the metal-oxygen reaction interface is some distance removed from the sample surface. The effect of high-velocity, high purity helium at 300 psi on the oxidation-evaporation relationship is not known.

Ideally, evaporation could be best controlled by the continuous transport of oxygen to the metal surface at a rate just sufficient to maintain oxide continuity and integrity without destructive oxidation or oxide spallation. At a 1 vpm total impurity level (16 μ partial pressure) in the helium, this condition might be fulfilled. It further appears that oxidation rates of the superalloys

tested would not be too severe at 2192 °F if the partial pressure of oxygen did not exceed a pressure of about 0.1 Torr. This value should be considered a maximum permissible oxygen pressure.

3) Haynes Alloy 25 exhibited much greater stability in oxygen atmospheres at 2048 °F than 2192 °F. The relative rate of attack by oxygen is comparable to the attack on Hastelloy X-280. From a gravimetric analysis, this would seem to indicate the interchangeability of these alloys at 2048°F.

4) At 1832 °F (1000 °C) the oxidation resistance of Hastelloy X-280, Haynes Alloy 25, and Hastelloy C are similar in atmospheres of 3 Torr oxygen pressure or greater. In general, however, Hastelloy X-280 seems to be more resistant to internal attack than Haynes Alloy 25 and also shows less dependence on surface preparation than either Haynes Alloy 25 or Hastelloy C.

5) All oxidized alloys tended to spall when cooled from the test temperatures, even in the case of rather thin films. Haynes Alloy 25 (the cobalt-base alloy) was especially susceptible to oxide spallation, particularly when the sample was thermally cycled. Hastelloy X-280 was more stable during thermal cycling, although in both cases more weight was lost from the sample by spalling than gained by oxidation. If Haynes Alloy 25 is to be used as a structural material in the ATR gas loop, cobalt bearing oxide particles can be expected to move within the coolant stream.

6) Other gaseous contaminants such as methane, carbon dioxide, carbon monoxide, and water vapor can be harmful if their concentration reaches a high enough level. The resulting effect, whether it be carburization or oxidation, will depend on the concentration of the various reactive gaseous species in the system. For example, methane alone in the system would be expected to carburize the superalloys. If oxygen is present in the system with the methane, the carburization reaction may not take place due to oxidation of the methane and/or the superalloys.

7) At 2192 °F, 100 Torr nitrogen pressure has no effect on Hastelloy X-280 and Haynes Alloy 25 except to inhibit evaporation.

8) In the case of a system free of oxidizing contaminants, metal vapors from potential evaporating structural materials will be present in the helium gas. This evaporation will be especially pronounced at temperatures in excess of 2000 °F. For example, at 2200 °F pure chromium has a vapor pressure of

about 10μ. In the event of an approach to equilibrium this chromium pressure would be comparable with the expected partial pressure of total contaminant ($\sim$ 1 vpm). The metal vapors must then be considered as potentially harmful as the expected gaseous contaminants (i.e., oxygen, carbon monoxide, carbon dioxide, nitrogen, hydrogen, etc.) in their deleterious effects on refractory metal irradiation specimens (solution and subsequent masking of irradiation effects).

9) In the case of Hastelloy X-280 - Haynes Alloy 25 weldments at 2192 ^{o}F, the oxidation resistance of the Haynes Alloy 25 will determine the oxidation resistance of the couple. Hastelloy X-280 - Hastelloy X-280 weldments show oxidation resistance equivalent to the parent metal.

10) Grade A helium has a corrosive effect on Haynes Alloy 25 and Hastelloy X-280 at 1900 ^{o}F (1038 ^{o}C). Hastelloy X-280 forms a more tenacious scale and exhibits less internal attack for a given exposure.

11) The superalloys tested exhibit extremely complex corrosion behavior as a function of oxygen pressure. At very low oxidant partial pressures (expected in the ATR loop), it is impossible to predict exactly what degradation phenomenon will be most important especially when the effects of high velocity, high pressure helium are not known. It is of utmost importance that a careful ATR structural material surveillance program be maintained. Samples which can be withdrawn and analyzed should be located within the loop in positions which offer the most favorable conditions for oxidation and evaporation. Weight change data, metallographic analysis, and, if possible, mechanical testing should be used in the evaluation of the surveillance samples.

EXPERIMENTAL

Materials

The composition of each superalloy used in the following tests is given in Table I. Hastelloy X-280 is a low cobalt form of Hastelloy X. Its oxidation resistance is assumed to be comparable to the more common Hastelloy X.

TABLE I

COMPOSITION OF SUPERALLOY SHEET STOCK, wt%

Material	Haynes 25	Hastelloy X-280	Hastelloy C	Inconel-600
C	0.12	0.10	0.07	0.06
Si	0.48	0.56	0.54	0.20
Mn	1.57	0.40	0.59	0.20
P	0.004	0.006	0.01	-
S	0.003	0.004	0.006	0.007
Cr	19.90	22.48	16.0	15.50
Co	Bal	0.28	2.0	0.09
Cu	-	-	0.03	0.10
Fe	1.28	17.96	5.0	6.50
Mo	-	8.53	16.0	-
Ni	10.18	49.18	Bal	76.50
V	-	-	0.25	-
W	14.76	0.50	3.75	-
Al	-	-	-	0.20
Ti	-	-	-	0.30

All metals were received in the solution-annealed and descaled condition. The thickness of the sheet stock varied from 30 to 60 mils depending on the alloy. Samples used for the weldment studies were obtained from separate one-fourth in. (0.635 cm) thick stock; however, no chemical analyses were available for these materials.

Coupon samples for the oxidation tests were rectangular, 1/2 by 2 in. (1.27 cm by 5.08 cm) having a three-sixteenths in. diam hole centered one-fourth in. from one end. Electropolished,* abraded on 0 paper and as-received samples were used to determine possible surface effects at 1832 ^{o}F (1000 ^{o}C). Samples used for tests at 2048 and 2192 ^{o}F (1120 and 1200 ^{o}C) were all abraded on 400X emery paper, then degreased.

---

* Electrolytic etch bath is 55 vol% H_3PO_4, 22 vol% H_2SO_4, 23 vol% H_2O. Current density of 1.2 amp/cm^2 for 6 min sufficed to produce good surface on all alloys tested.

The gas atmospheres used in the bulk of the tests were of "research grade" or equivalent purity. Tests made using a continually flowing gas stream were done using commercial purity gases. Distilled water with the dissolved gases removed was used as the source of water vapor.

Static Microbalance Tests

All oxidation or evaporation data which permitted graphical analysis of weight change as a function of time for an individual sample were obtained by use of an Ainsworth semimicro recording balance, Model RV-AU-1, completely enclosed in a vacuum system. Figure 1 is a schematic representation of the equipment used. At oxygen pressures in excess of 3 Torr,

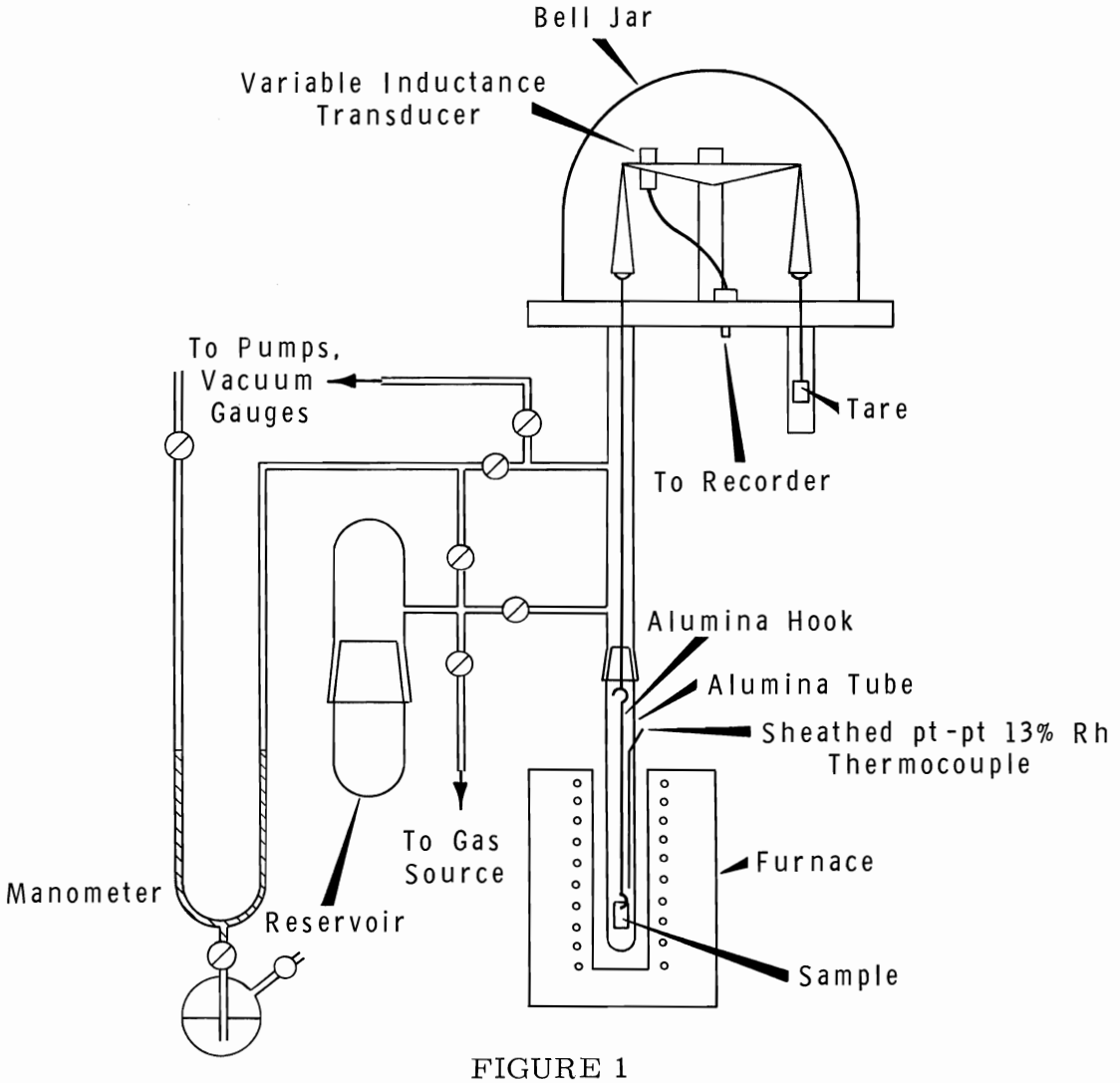

FIGURE 1

Schematic Diagram of Balance and Associated Vacuum Equipment

the balance chamber, reservoir, and furnace tube contain the static atmosphere employed during the test. For oxygen pressures less than 3 Torr, an oxygen leak from an external source was adjusted while vacuum is being continuously imposed on the system in order to maintain the desired pressure. These tests may still be considered static. Tests run at 2192 ^{o}F and at pressures less than 3 Torr were done in a static unrefreshed system. The consumption of oxygen was followed by pressure measurements and, in general, is indicated for each test on the respective curve.

Test samples for the 2192 and 2048 ^{o}F runs were suspended on an alumina hook within a high density, low permeability alumina furnace tube. In the 1832 ^{o}F tests, both hook and tube were made of quartz. The hook was suspended from the balance arm by means of a fine tungsten wire or a gold chain. To initiate an oxidation run, the furnace tube and balance chamber was evacuated to 10^{-5} Torr. The sample was then brought to the desired test temperature in vacuo by raising a preheated resistance furnace around the furnace tube. When the sample attained the desired temperature, the atmosphere (if one was desired) was admitted to the furnace tube, and weight changes were continuously recorded.

The temperature of the sample was monitored by means of a platinum sheathed Pt - Pt 13% Rh thermocouple enclosed within the furnace tube, and located near the sample.

Thermal Cycling Tests

The recording microbalance system was used to monitor the effects of heating and cooling on Haynes Alloy 25 and Hastelloy X-280 samples in a static oxygen atmosphere. Each cycle consisted of a 3000 min oxidation at temperature (2048 ^{o}F) followed by a furnace cooling to room temperature. The oxidizing atmosphere was maintained during the cooling process. The cooling time consisted of approximately 2 hr for the temperature to drop from 2048 to 950 ^{o}F, followed by an additional 3 to 4 hr to reach room temperature.

At the completion of each cycle, the sample was taken from the balance chamber, brushed to remove loose oxide, weighed, and then replaced. Each cycle represents a standard static microbalance test.

Weldment Tests

Samples of superalloy weldments of Hastelloy X-280 and Hastelloy X-280 (Hastelloy X-280 filler wire), Hastelloy X-280 and Haynes Alloy 25 (Hastelloy W filler wire), and Haynes Alloy 25 and Haynes Alloy 25 (Haynes Alloy 25 filler wire) were obtained for corrosion testing.* A description of the welding procedure (TIG) has been published.[4]

The welds were made in 0.25 in. (0.635 cm) thick plate, which was machined to a thickness of 0.1 in. (0.25 cm) and abraded on 240X emery prior to corrosion testing. Sample coupons were 0.5 in. wide and 1.5 in. long.

The samples were suspended on an alumina rod in a high temperature tube furnace and exposed to flowing contaminated helium (He + 0.5% O_2 + 0.54% N_2) at 2192 ^{o}F (1200 ^{o}C) for seven days. Gas flow was maintained at 0.5 scfh.

Tests in Grade A Helium at 1900 ^{o}F (1038 ^{o}C)

Two separate tests were conducted to determine the corrosive effect of Grade A helium on Haynes Alloy 25 and Hastelloy X-280 at 1900 ^{o}F.

For each test, six samples of the alloy sheet (as-received, degreased) were cut to 1 by 1 1/4 in. (2.54 by 3.18 cm) dimensions and placed in a quartz reaction tube. The samples were bent in such a manner that the gas stream was divided, half the gas passing over each major surface of the test coupon.

Each set of coupons was exposed to Grade A helium flowing at a linear rate of about 2 in./sec for 10 days, a sufficient time to almost exhaust a standard 1A bottle of helium. The helium employed had an analyzed purity of 99.97%. The water vapor content was not included in the analysis, and so is unknown.

---

* Courtesy of R. L. Knecht, Pacific Northwest Laboratory

RESULTS AND DISCUSSION

Oxidation at 1832 °F (1000 °C)

The oxidation behavior of Hastelloy X-280, Haynes Alloy 25, and Hastelloy C was determined at 1832 °F as a function of oxygen pressure and surface preparation. Weight gain curves were obtained from the recording microbalance. These curves, when transcribed from the recorder chart, represent a continuous determination of weight change.

Figure 2 shows a band of weight gain curves for oxidized Hastelloy X-280 in the as-received, electropolished, and abraded (0 paper) conditions. Each condition of the alloy was oxidized in untreated air, 25 Torr oxygen, and 3 Torr oxygen pressure. It appears that the oxidation kinetics of Hastelloy X-280 are not significantly influenced by sample preparation or oxygen partial pressure, within the limits employed.

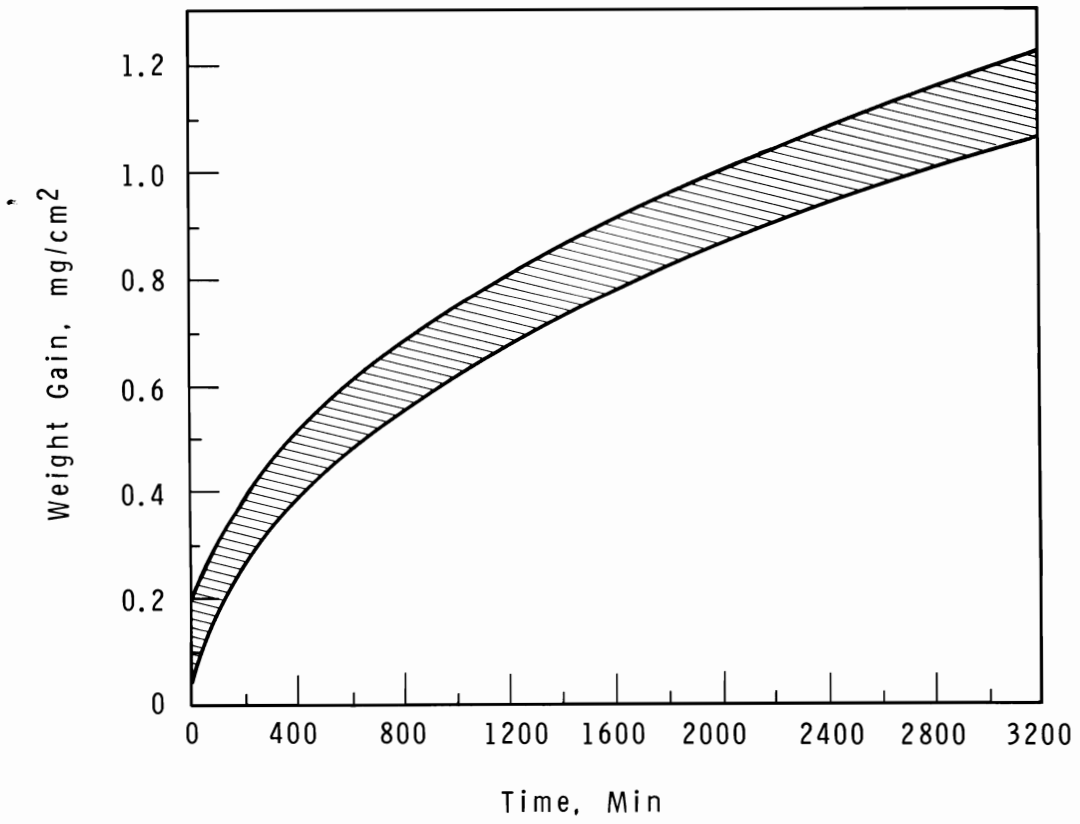

FIGURE 2

Oxidation of Hastelloy-X at 1832 °F (1000 °C)

The oxidation behavior of Haynes Alloy 25, a high strength cobalt-base alloy is shown in Figure 3. There appears to be no clear-cut effect of surface treatment on the oxidation rate, but a pronounced dependence on oxygen pressures does exist. At 1832 °F, Haynes Alloy 25 shows an oxidation behavior similar to that of Hastelloy X-280 on the basis of weight gain measurements only. It must be borne in mind that the manner of oxidation (i. e., uniform, uneven, internal, or intergranular) has a profound influence on the load carrying capability of a superalloy structure so that weight gain measurements alone will not qualify a superalloy for a given service. At a given test temperature, weight gain measurements will give an excellent first indication of the oxidation resistance of a given alloy, as well as the effect of surface preparation and variation of oxidant pressure on the oxidation resistance.

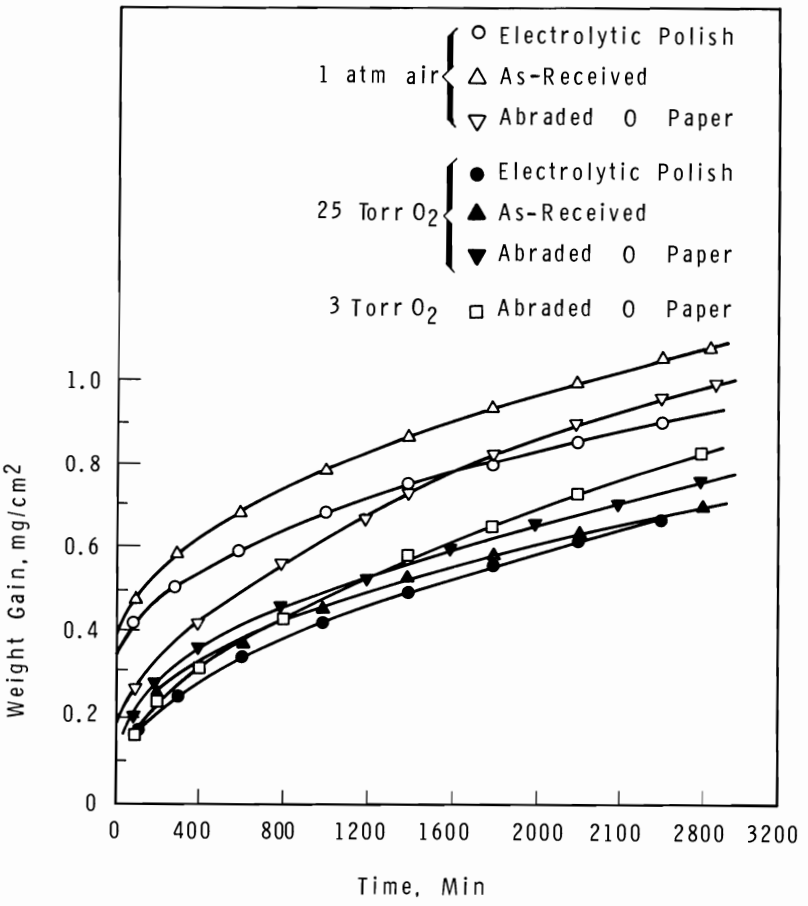

FIGURE 3

Oxidation of Haynes 25 at 1832 °F (1000 °C)

Figure 4 shows that Hastelloy C is even more oxidation resistant than Hastelloy X-280 under the given test conditions, though the oxidation behavior of Hastelloy X-280 appears to be more consistent. The unusual weight gain curve at 25 Torr oxygen pressure for as-received material was found to be reproducible. Pressure has a significant effect on the as-received material, but has little effect if the surface is abraded.

Although Hastelloy C does show good oxidation resistance, it cannot be considered a first candidate for ATR structural applications, because of its comparatively low strength at high temperature.

The 1832 ^{o}F test data shows that the corrosion resistance of Haynes Alloy 25 and of Hastelloy X-280 is comparable from a weight gain standpoint. However, Simenz [5] graphically illustrates the superiority of Hastelloy X over Haynes Alloy 25 in air for 10 hr at temperatures between 1600 and 2200 ^{o}F on the basis of metallographic analyses. At 1830 ^{o}F, he reports 0.6 mil metal "affected" after 10 hr in air for Hastelloy X, opposed to 1.3 mils "affected" in the case of Haynes Alloy 25. Wlodek, [6, 7] in his studies of the oxidation behavior of Rene 41, U-700, and Hastelloy X,

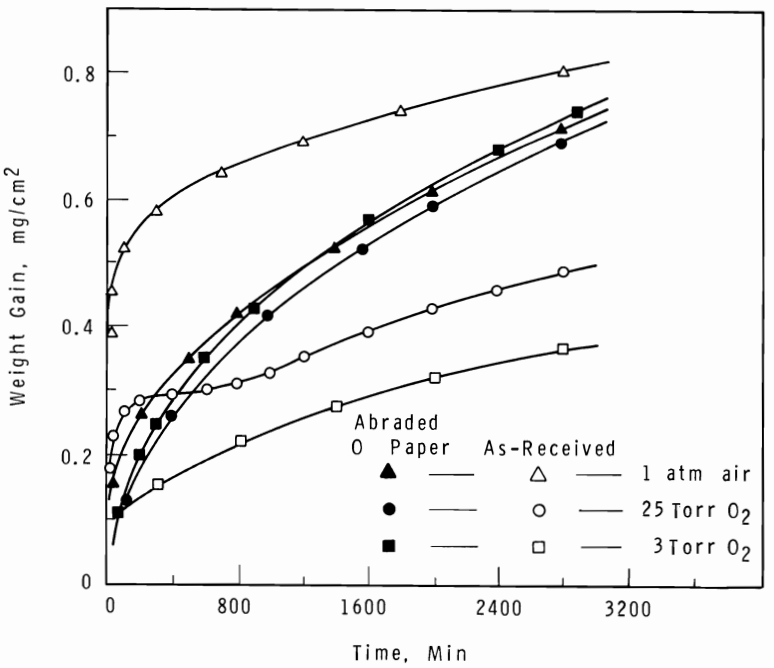

FIGURE 4

Effect of Oxidant Pressure and Surface Preparation on Oxidation of Hastelloy C at 1832 ^{o}F (1000 ^{o}C)

concludes that internal oxidation is more serious than scale induced effects in promoting failure in components undergoing dynamic loading, and illustrates the superior resistance of Hastelloy X to internal oxidation and alloy depletion.

Oxidation at 2048 °F (1120 °C)

The corrosion data for the 2048 °F and 2192 °F tests were obtained from samples abraded on 400X emery paper as the only surface preparation.

Figures 5, 6, 7, and 8 show the weight gain as a function of time for Hastelloy X-280 and Haynes Alloy 25. As indicated by the 1832 °F tests, the general shape of the curves appear to be parabolic. These weight gain data plotted as a parabolic function ($[\Delta \text{Weight/Area}]^2$ versus time), Figures 9 and 10, indicate that there are two regions at which different parabolic rate constants are operative. Table II lists the calculated rate constants and their approximate region of applicability.

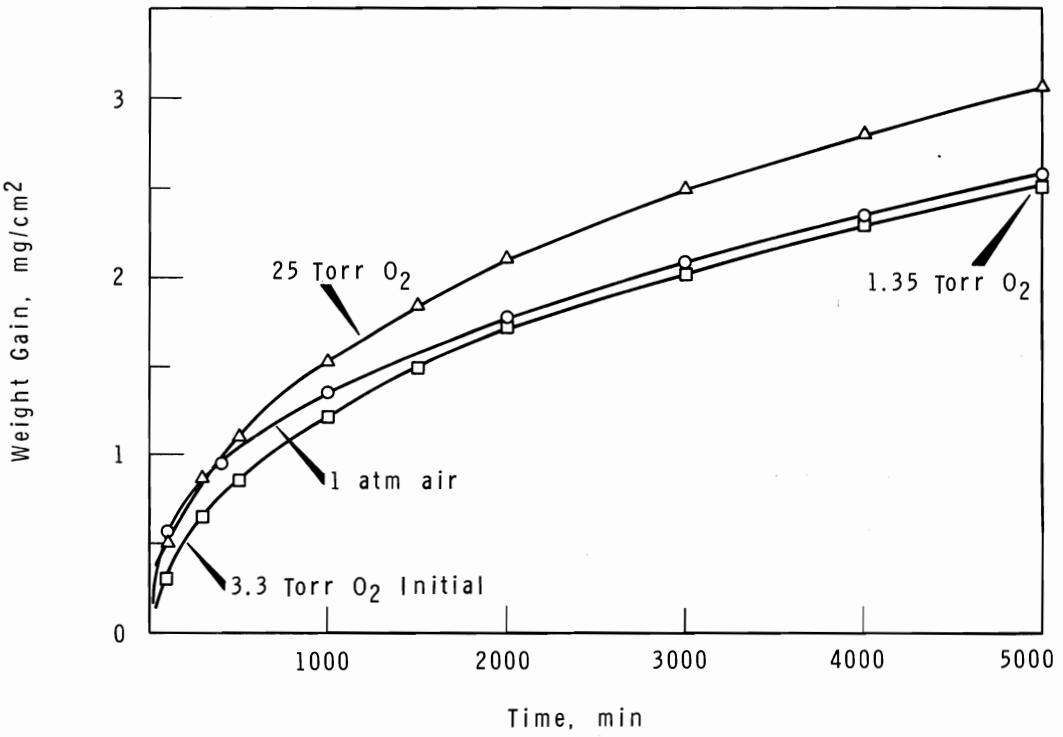

FIGURE 5

Oxidation of Hastelloy X-280
in a Static Gas System at 2048 °F (1120 °C)

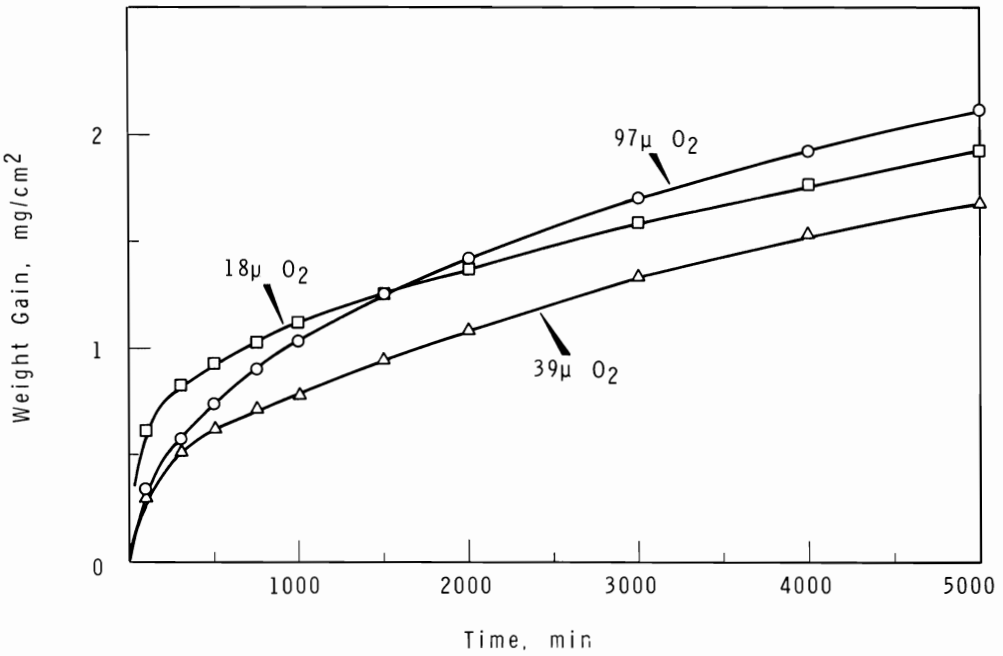

FIGURE 6

Oxidation of Hastelloy X-280
in a Replenished Gas System at 2048 °F (1120 °C)

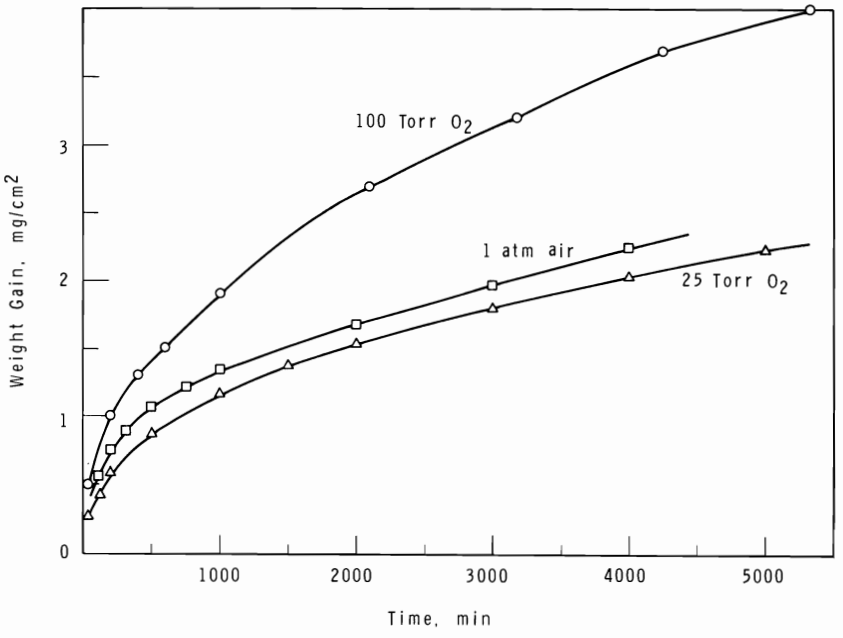

FIGURE 7

Oxidation of Haynes 25
in a Static Gas System at 2048 °F (1120 °C)

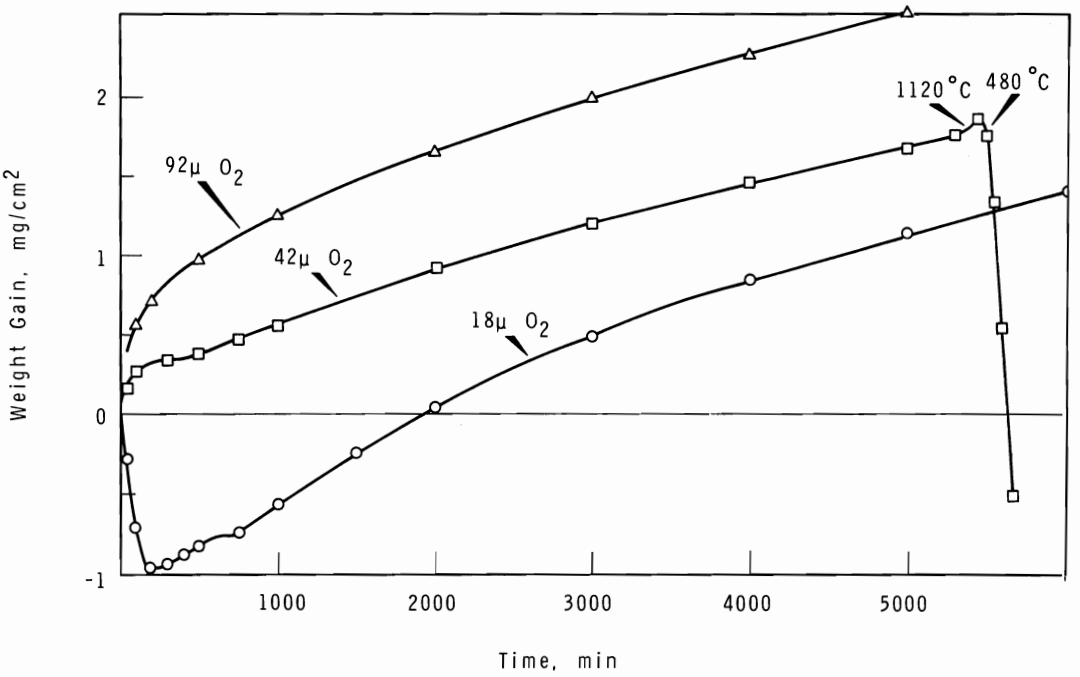

FIGURE 8

Oxidation of Haynes 25
in a Replenished Gas System at 2048 °F (1120 °C)

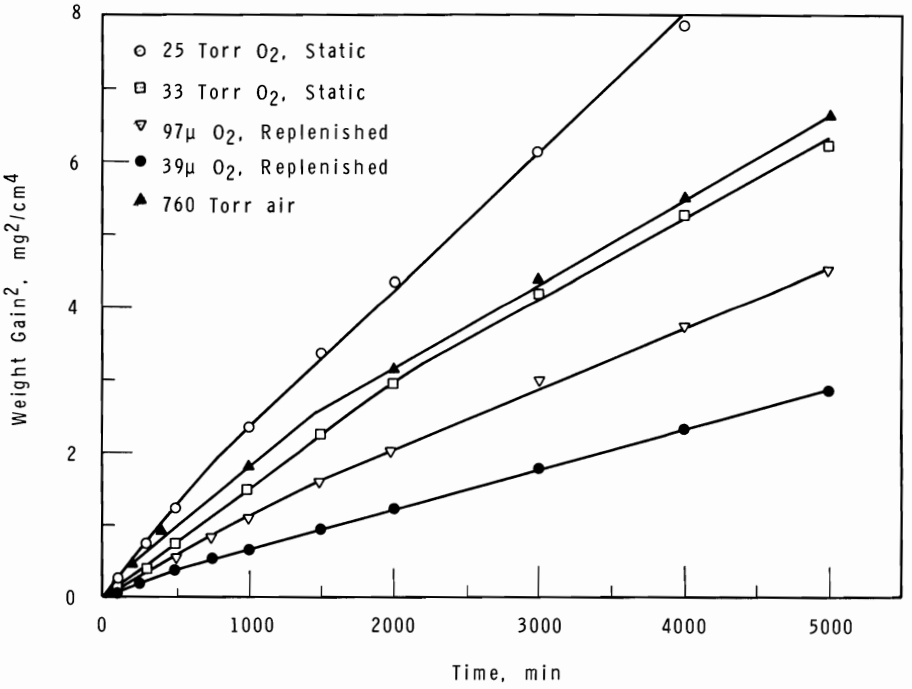

FIGURE 9

Parabolic Oxidation of Hastelloy X-280 at 2048 °F

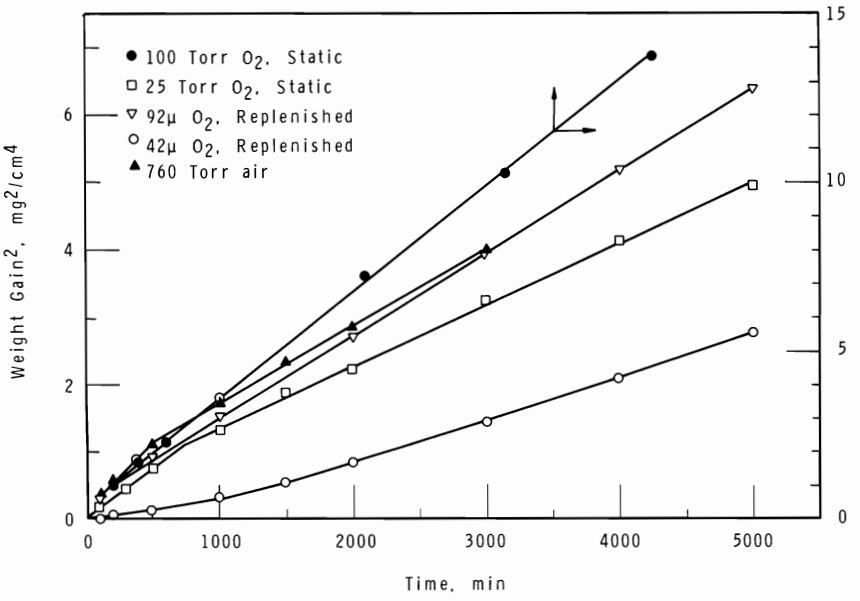

FIGURE 10

Parabolic Oxidation of Haynes Alloy 25 at 2048 °F

TABLE II

PARABOLIC RATE CONSTANTS AT 2048 °F

Alloy	Atmosphere	Rate mg^2/cm^4 sec	Applicable Region, min
Hastelloy X	25 Torr oxygen	4.14×10^{-5}	<750
		3.10×10^{-5}	>750
	3.3 Torr oxygen	2.53×10^{-5}	<2000
		1.88×10^{-5}	>2000
	97 μ oxygen	1.83×10^{-5}	<1250
		1.45×10^{-5}	>1250
	39 μ oxygen	9.16×10^{-6}	>250
	1 atm air	2.66×10^{-5}	<1500
		1.94×10^{-5}	>1500
Haynes Alloy 25	100 Torr oxygen	5.38×10^{-5}	250 to 4000
	25 Torr oxygen	2.38×10^{-5}	<750
		1.51×10^{-5}	>750
	92 μ oxygen	2.05×10^{-5}	500 to 5000
	42 μ oxygen	1.09×10^{-5}	2000 to 5000
	1 atm air	3.2×10^{-5}	<500
		1.66×10^{-5}	>500

Wlodek [6] studied the oxidation of Hastelloy X in dry air and arrived at curves similar to the ones shown. At 2000 °F (1093 °C) he calculated parabolic rate constants of 2.85×10^{-5} mg^2/cm^4 sec for times less than 400 min and 1.35×10^{-5} mg^2/cm^4 sec for times greater than 400 min.

Though the present work is not as detailed as Wlodek's, the agreement between the two investigations permits extrapolation of the present data with some confidence. If the rate constants operative after some length of time are used, an approximate pressure dependence for these alloys can be determined. A log-log plot of rate versus oxygen pressure for Hastelloy X-280 (Figure 11) shows an oxidation rate dependent on the one-fifth power of the oxygen pressure. Haynes Alloy 25 gave such a random data scatter that no numerical value could be determined for the oxygen pressure dependence. However, the weight gain curves (Figures 7 and 8) indicate a slight rate increase with oxygen pressure.

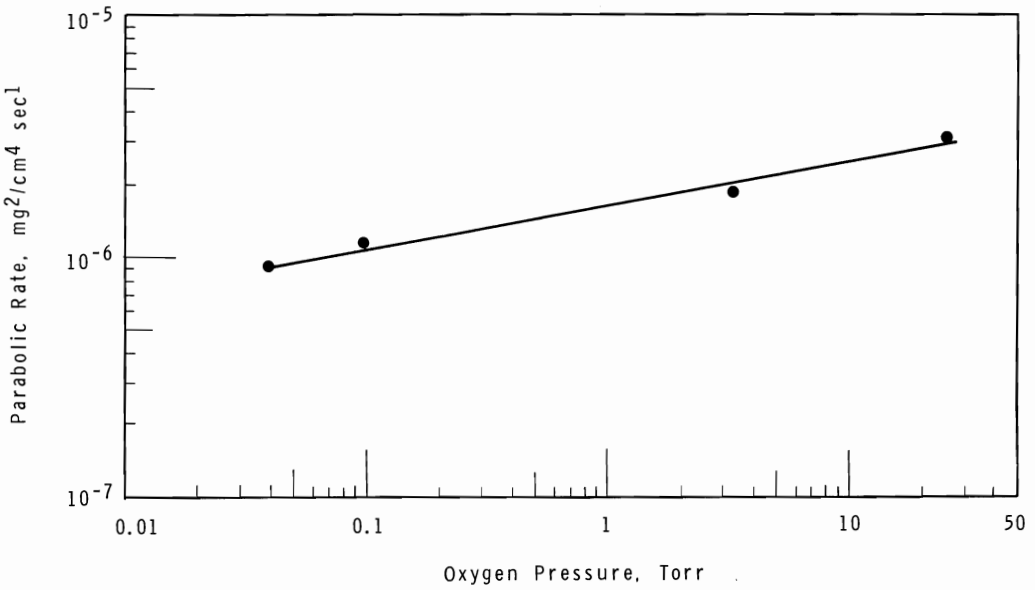

FIGURE 11

Oxygen Pressure Dependence for Hastelloy X-280 at 2048 °F

Oxidation at 2192 °F (1200 °C)

The oxidation behavior of the superalloys at 2192 °F was approached with the intent to determine the oxidation resistance retained by alloys subjected to a corrosive atmosphere at this high temperature. Figures 12, 13, and 14 show the weight gain results for Hastelloy X-280, Haynes Alloy 25, and Inconel 600.

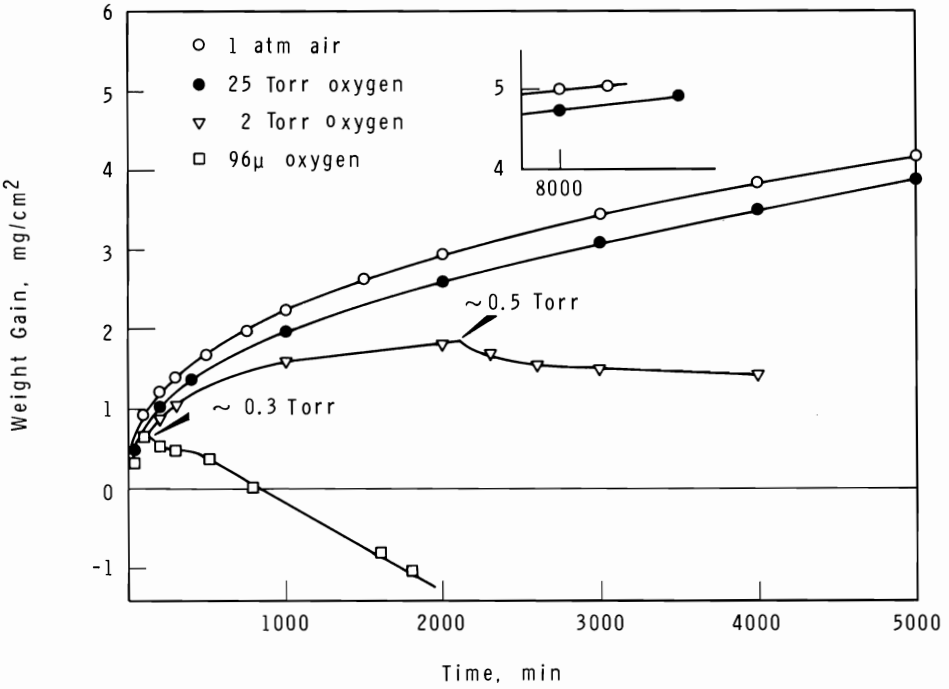

FIGURE 12

Oxidation of Hastelloy X-280 at 2192 °F (1200 °C)

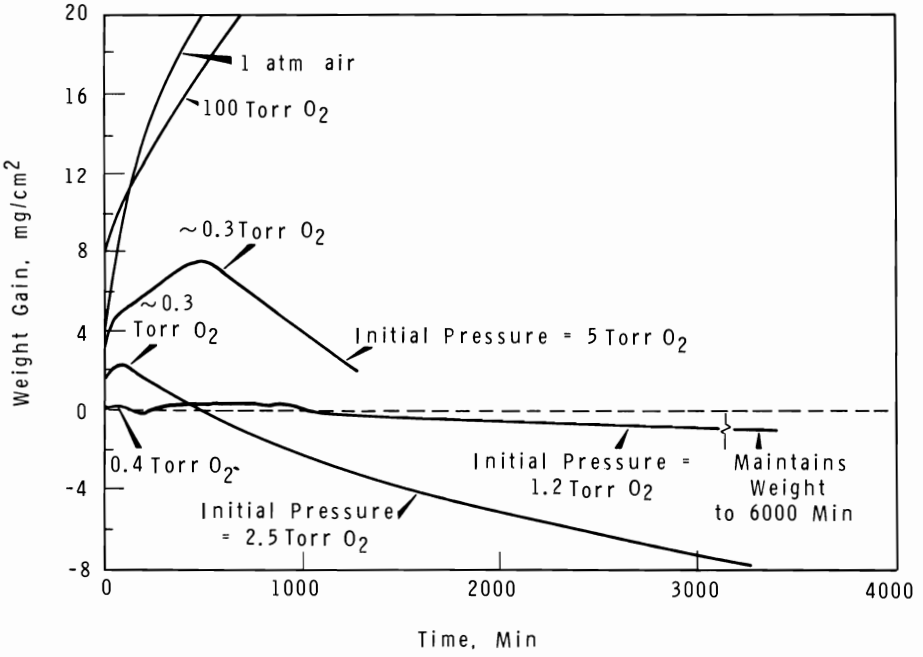

FIGURE 13

Oxidation of Haynes 25 at 2192 °F (1200 °C)

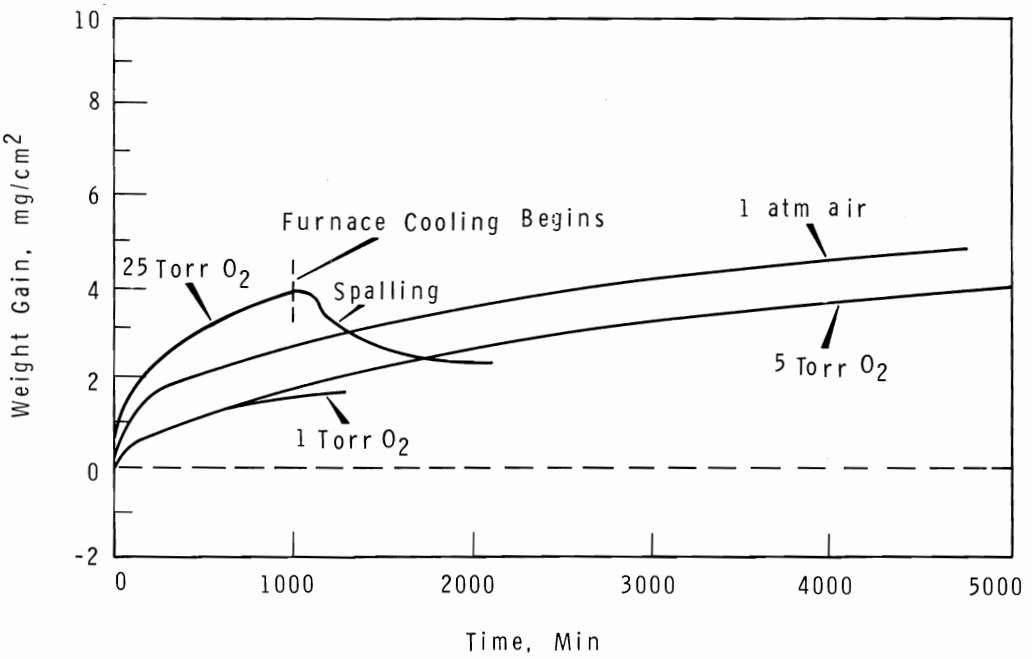

FIGURE 14

Oxidation of Inconel 600 at 2192 °F (1200 °C)

Because the oxygen atmosphere is unreplenished in these tests, the oxidation reaction will cause a continuous diminution of pressure in the system. This loss of pressure is not important when the initial pressure is 25 Torr or greater. For Hastelloy X-280 in a system with an initial pressure of 2 Torr oxygen, the pressure in the system fell to about 0.5 Torr oxygen in 2200 min (Figure 9). There was no further gain in weight beyond that point, indicating a virtual halt in the oxidation process. When the sample was cooled, oxide spalling occurred. At the end of the test, the sample was found to be still coated with a continuous, tenacious oxide film which completely covered the sample. When the pressure in the system at the beginning of a test was 0.9 Torr oxygen, the halt in weight gain occurred at a system pressure of 0.3 Torr, within 100 min. In this case, the thin oxide film was not continuous and tenacious enough to protect the sample from evaporation which along with (presumed) oxide spallation, caused a continuing weight loss.

Haynes Alloy 25 under similar conditions (Figure 14) shows a rapid oxidation in air or 100 Torr oxygen at 2192 °F. When the initial system pressure was 5 Torr oxygen or less, the oxidation reaction removed gaseous

oxygen from the system until a system pressure of approximately 0.3 Torr was attained. At this time, the oxide lost its coherency, and spallation of the oxide caused the sample to lose weight.

The samples which have undergone testing at 5 and 2.5 Torr initial oxygen pressures have a duplex oxide. The outer film is not adherent and apparently gives rise to the spalling observed. The sample oxidized at an initial pressure of 1.2 Torr oxygen, however, did not show the duplex film structure at the completion of the run but did show remarkable stability during the course of the run.

The oxidation behavior of Inconel 600 is shown in Figure 14. Note that there is not a clear-cut pressure effect. Spalling of the oxide occurs on cooling from the test temperature. Weight gains of Inconel 600 and Hastelloy X-280 are similar at 2192 ^{o}F. Because of this similarity, it was decided that the bulk of the testing should only deal with alloys of a different base metal, i.e., the nickel-base Hastelloy X-280 and the cobalt-base Haynes Alloy 25. Also, these two superalloys are most likely to be adopted in the construction of the ATR gas loop.

Thermal Cycling Effect

Stresses within an oxide resulting from phase changes or from differences between the oxide and the metal substrate during heating and cooling cycles can cause spalling of a protective oxide film and subsequent increased corrosion of the base metal. Tests were made on Hastelloy X-280 and Haynes Alloy 25 in a severe oxidizing atmosphere, 25 Torr oxygen, to follow the effect of thermal cycling from room temperature to 2048 ^{o}F (1120 ^{o}C) on the oxidation process. Figures 15 and 16 show graphically the effect of nine such heating and cooling cycles.

The oxidation behavior of Haynes Alloy 25 was strongly influenced by thermal cycling. Gross spalling of the surface oxide undoubtedly added to the increased oxidation in the latter cycles. The most severe spalling on cooling occurred for both alloys as the temperature dropped to approximately 900 ^{o}F.

The weight change shown in Figure 16 for Haynes Alloy 25 is not the actual weight change for the sample. Mechanical brushing of the coupon

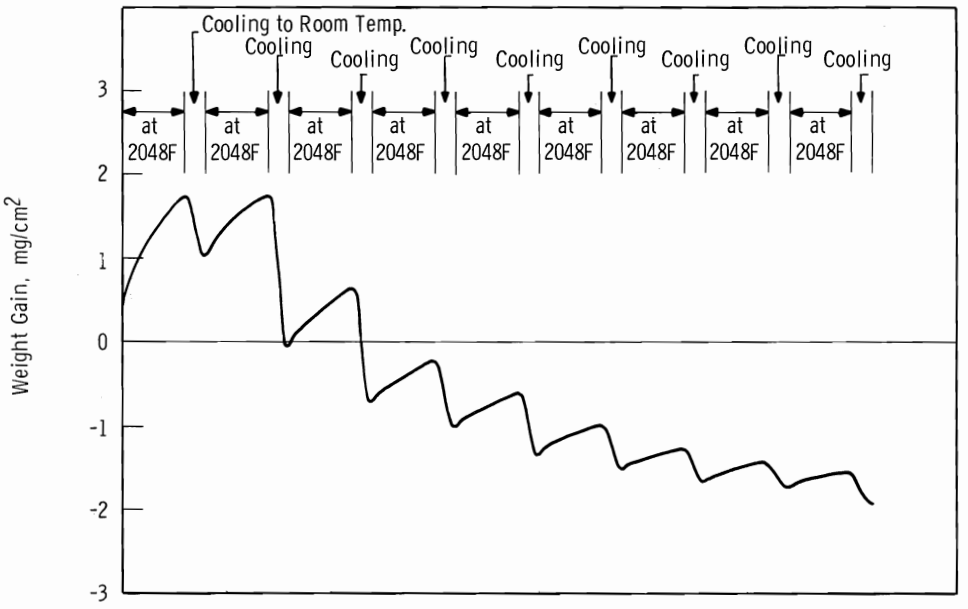

FIGURE 15

Thermal Cycling of Hastelloy X-280 Static Test in 25 Torr O_2

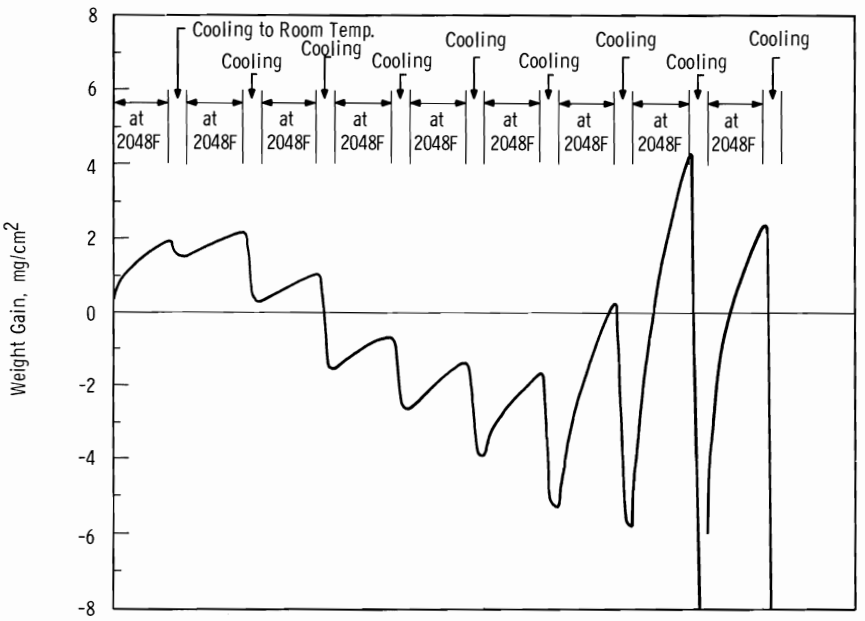

FIGURE 16

Thermal Cycling of Haynes Alloy 25 Static Test in 25 Torr O_2

between cycles and the severe spalling which exceeded the capacity of the microbalance at the end of the eighth and ninth cycles contributed to the total weight loss. Sample weights independently obtained on a second microbalance show that the curve is only a relative picture of both weight loss and weight gain because spallation can occur during both heating and cooling. The curve for Hastelloy X-280 is an accurate representation of both weight gain and weight loss. Note also that the oxidation rate of Hastelloy X-280 continually decreases while that of Haynes Alloy 25 starts to increase after the fifth cycle.

The total metal weight loss for the nine cycles from Hastelloy X-280 was 3 mg/cm^2 due to spalling with an additional 8.1 mg/cm^2 metal remaining on the coupon as oxide. Haynes Alloy 25 lost 62 mg/cm^2 due to spalling while 21 mg/cm^2 metal remained on the sample as oxide. The total metal weight loss amounts to a metal penetration of 0.58 mil for Hastelloy X-280 and 3.57 mils for Haynes Alloy 25, assuming uniform oxidation and neglecting intergranular penetration.

Limited data was also obtained for Haynes Alloy 25 thermally cycled in a 20μ replenished oxygen atmosphere. The oxidation, as expected, was less severe; however, the spalling characteristics were similar to those observed in the 25 Torr oxygen test. It is apparent that even for thin films spalling will occur, and thus particulate matter should be expected in the ATR Loop in the event the superalloys oxidize.

Metallography shows the microstructure of both alloys at the completion of the ninth cycle (Figure 17). In addition, surface structures are shown. Crystal colonies can be noted on the Haynes Alloy 25, and the irregular attack of oxygen on the alloy can also be noted.

GENERAL DISCUSSION:

Kubaschewski and Hopkins [8] have recently outlined the general theory of alloy oxidation. If a nickel-chromium alloy contains more than 15 wt% chromium, the oxide growth is reported to be due to predominant formation of Cr_2O_3 or $NiO\text{-}Cr_2O_3$. Hauffe (as reported by Kubaschewski)

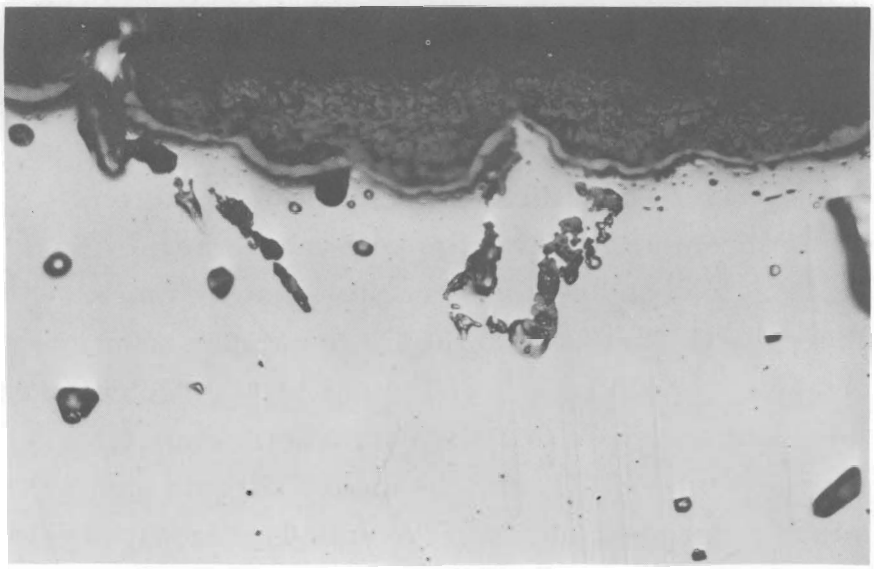

Haynes Alloy 25 in 25 Torr Oxygen
450 hr Exposure at 2048 °F
500X
Etchant: HCl - H_2O_2
46519B

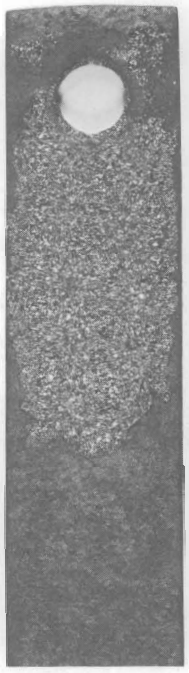

Haynes Alloy 25
2X 46519A

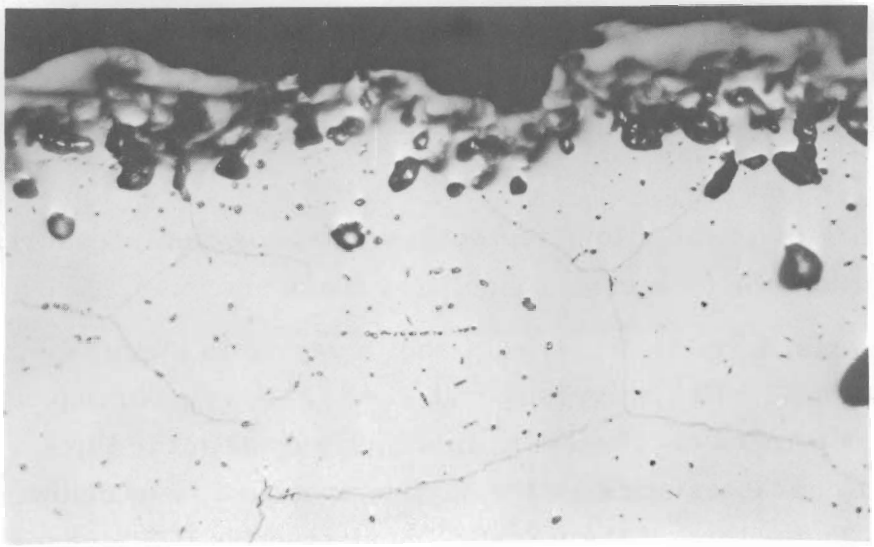

Hastelloy X-280 in 25 Torr Oxygen
450 hr Exposure at 2048 °F
500X
Etchant: HCl - H_2O_2
46518B

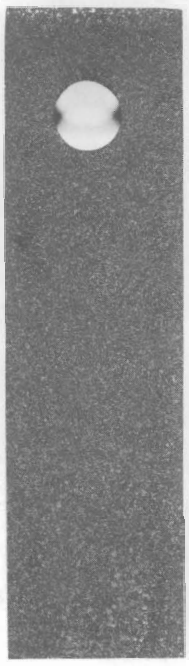

Hastelloy X-280
2X 46518A

FIGURE 17

Thermal Cycling of Hastelloy X-280 and Haynes Alloy 25

attributes the good oxidation resistance to the formation of the spinel. The oxidation is thought to be determined by the diffusion of Cr^{+3} ions across the scale. Caplan and Cohen [9] state that the evaporation of chromium oxide at 1000 to 1200 °C occurs by the oxidation of Cr_2O_3 to CrO_3 which evaporates from the surface. In the gas phase, CrO_3 dissociates back to Cr_2O_3 and redeposits. The depletion of chromium below a limiting value where NiO may predominate in the oxide scale has been observed to cause an increase in oxidation rate. This increase is attributed to the large number of lattice vacancies at the oxide surface.[8] Wlodek,[6] who studied the more complex Hastelloy X alloy, concludes that the scale initially consists of amorphous silicon dioxide which is overgrown by Cr_2O_3 and the nickel-chrome spinel. The spinel remains the minor constituent although the spinel colonies increase with time and temperature.

The oxidation resistance of cobalt alloys containing more than 9 wt% chromium is superior to alloys containing less chromium. The oxide formed is predominantly CoO with some CoO-Cr_2O_3. As the chromium content increases from 9 to 25 wt%, the oxidation resistance increases. The comparatively poor oxidation resistance of cobalt-chromium alloys containing less than 9 wt% as in the case of nickel is attributed to the large number of lattice vacancies at the surface.[8]

The oxidation behavior of the alloys tested in various oxygen pressures reveal a complex interaction among metal, oxide, and atmosphere.

In the case of Haynes Alloy 25, it appears that a very thin oxide film, such as that formed at 2048 °F in 18 μ oxygen or at 2192 °F in 1.2 Torr initial oxygen pressure, can be protective. However, in a static system the thicker films lose their adherent characteristics as the oxygen pressure falls below about 0.3 Torr oxygen. The nature of the thicker, nonprotective film suggests that a portion of the film undergoes a phase change at the low oxygen pressures. This phase change could promote degradation of the film as a whole and allow microscopic spallation to occur. The films formed at lower pressures under replenished conditions or in static systems at higher system pressures than approximately 1 Torr apparently do not undergo the degradation process, and film continuity is maintained.

In the case of Hastelloy X-280, the films formed in the low pressure, replenished oxygen atmospheres appeared protective at 2048 °F. Similarly, the film formed in 2 Torr oxygen at 2192 °F maintained continuity and protected the metal. However, the film formed in 0.9 Torr static oxygen at 2192 °F was not protective. The reasons for this oxygen pressure (or quantity) dependence is not clear.

The protective and nonprotective nature of the oxide layer is graphically shown for Hastelloy X-280 at 2192 °F (1200 °C) in Figure 18. A coupon sample was exposed to a continuously replenished atmosphere of air at about 10 μ pressure. During the first 15 hr of exposure, a steady weight loss was observed due to the evaporation mechanism (region A). During this period the metal-oxygen reaction was not occurring to any extent on the metal itself. After 15 hr the decreasing evaporation rate apparently allowed the oxidation reaction to begin on the sample surface, which was quickly coated with oxide. At this time a discontinuity appeared in the weight change curve, and weight gain began at a rate commensurate with the availability of oxygen in the system. At 40 hr time high vacuum conditions were imposed, and the oxidation rate decreased. The very thin oxide formed during period B retained its protective nature during the high vacuum conditions, preventing evaporation.

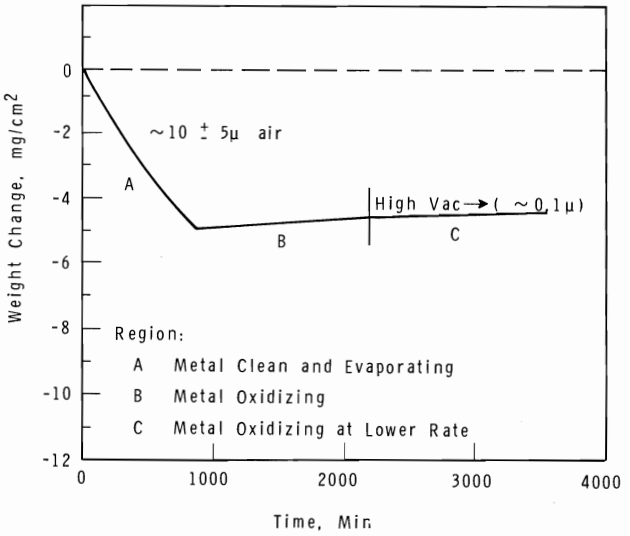

FIGURE 18

Hastelloy X Behavior, 2192 °F (1200 °C) at Low Air Pressures

These results seem at variance with earlier results (Figure 12), in which a thin film formed on Hastelloy X-280 (initial pressure = 0.9 Torr) quickly lost its protective nature and allowed evaporation to proceed. The explanation may lie in variable metal surface composition and texture in the two cases. In one case (Figure 12) the oxide formed on essentially as-received Hastelloy X-280 abraded on 400X emery; whereas, in the second case (Figure 18), the oxide film formed on Hastelloy X-280 of a different surface composition (lower chromium and concentrated nonvolatiles) and different texture, i.e., convolute in appearance.

Thus a single general remark covering the protective nature of the oxide will not suffice. Consideration must be given to many variables that can affect the nature of the oxide film.

Metallographic analysis (Figures 19 through 22) was used to examine the surface oxide and to determine the degree and type of penetration into the bulk metal. Both Haynes Alloy 25 and Hastelloy X-280 appear resistant to gross internal oxidation and intergranular penetration. The overall oxidation of Haynes Alloy 25 at 2192 ^{o}F in moderate oxygen pressures is so rapid, however, that it would be meaningless to speak of various modes of oxide penetration.

Question has been raised as to the nature of the voids seen in the micrographs. Evidence exists that these voids are filled during the oxidation process and that the inclusions are lost during metallographic analysis.[11]

Corrosion by Carbon Oxides and Water Vapor

The previous section considered the reaction between metal and oxygen. Experience with a high temperature, high velocity gas loop (Dynamic Materials Testing Apparatus, DMTA) has indicated water vapor to be a primary contaminant in a pure helium gas stream.[12, 13] Traces of other contaminants, such as methane, nitrogen, and oxygen, have also been observed. This and the following sections will consider other forms of attack which could affect the structural material in the ATR gas loop.

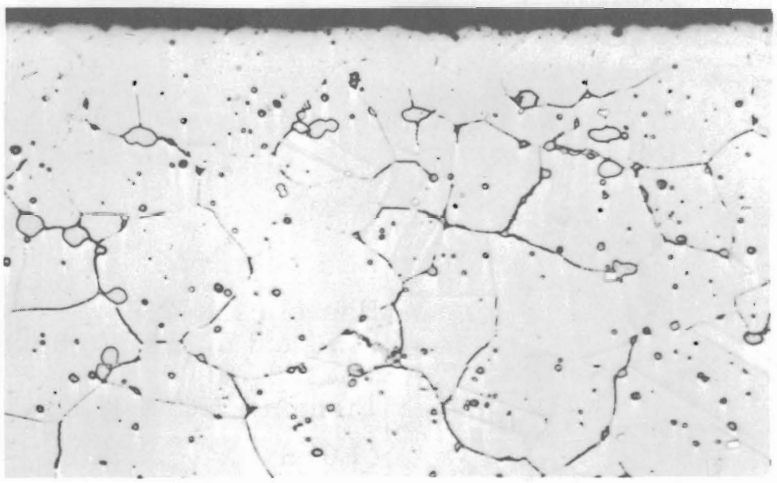

Hastelloy X-280
Etchant: HCl - H_2O_2
4L68

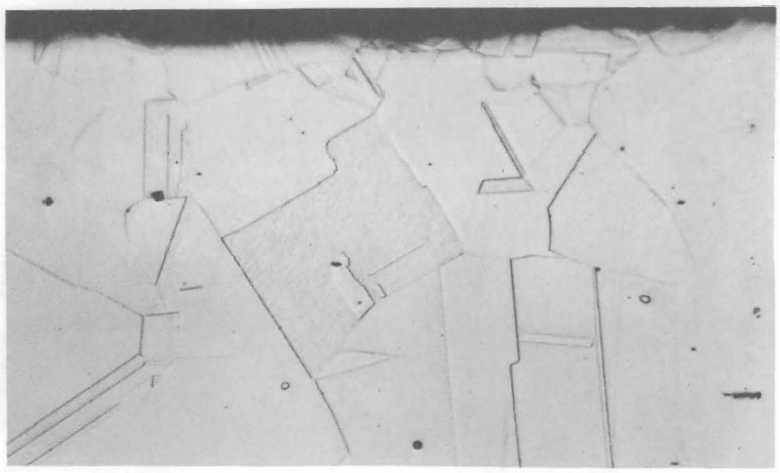

Haynes Alloy 25
Etchant: HCl - H_2O_2
4L71

Inconel 600
Etchant: 97 HCl - 3 HNO_3 - 5 H_2SO_4
4L72

FIGURE 19

As-Received Alloy Samples

500X

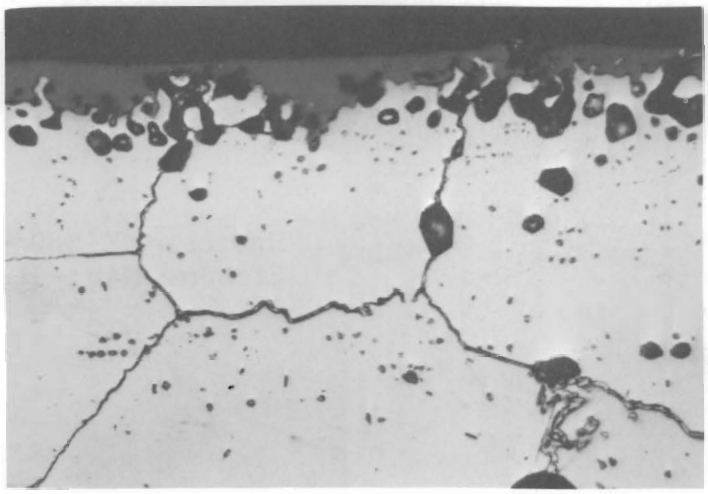

Hastelloy X-280
Oxidized in air, 78 hr
at 2192 °F
Etchant: HCl - H_2O_2
4L66B

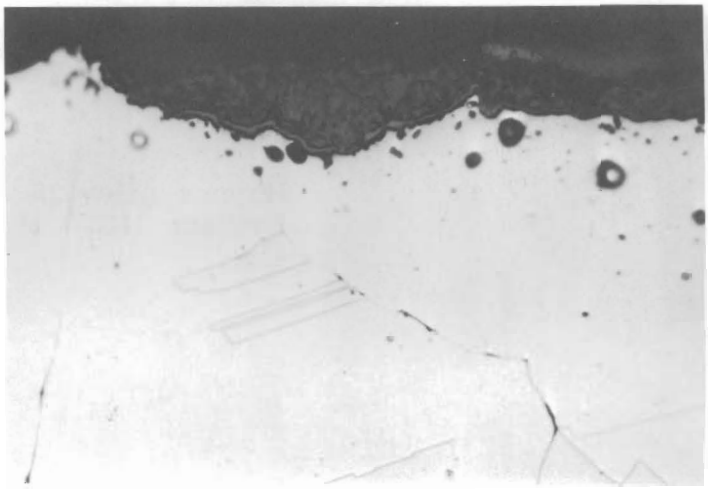

Haynes Alloy 25
Oxidized in air, 6 hr
at 2192 °F
Etchant: 97 HCl - 3 HNO_3 -
5 H_2SO_4
4L69

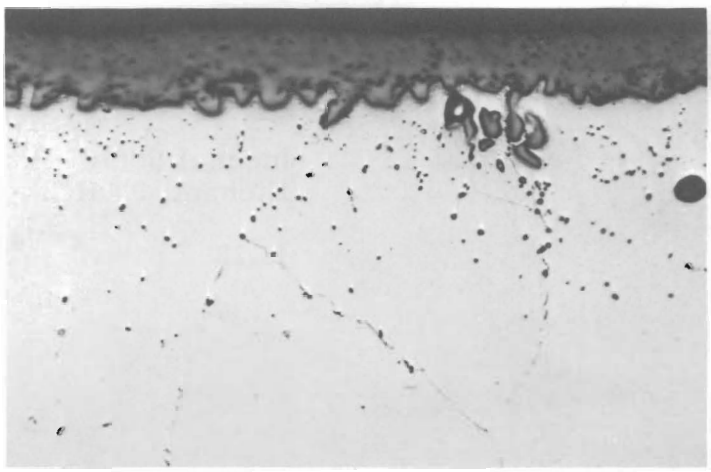

Inconel 600 Oxidized
in air, 75 hr at 2192 °F
Etchant: 97 HCl - 3 HNO_3 -
5 H_2SO_4
4L74

FIGURE 20

Oxidation of Superalloys in Air at 2192 °F

500X

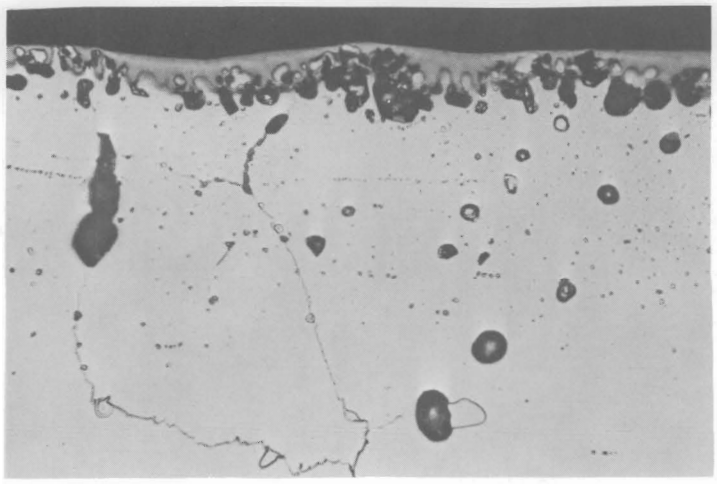

1 atm air 84 hr exposure
Etchant: HCl - H_2O_2
4L1524

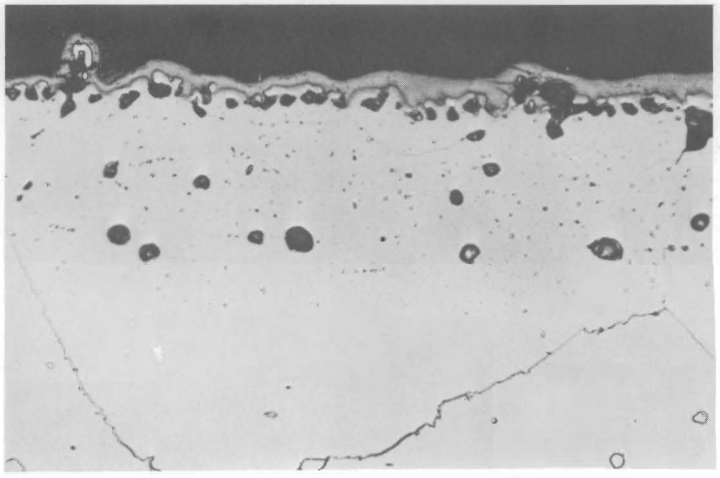

97 μ oxygen
84 hr exposure
Etchant: HCl - H_2O_2
4L1527

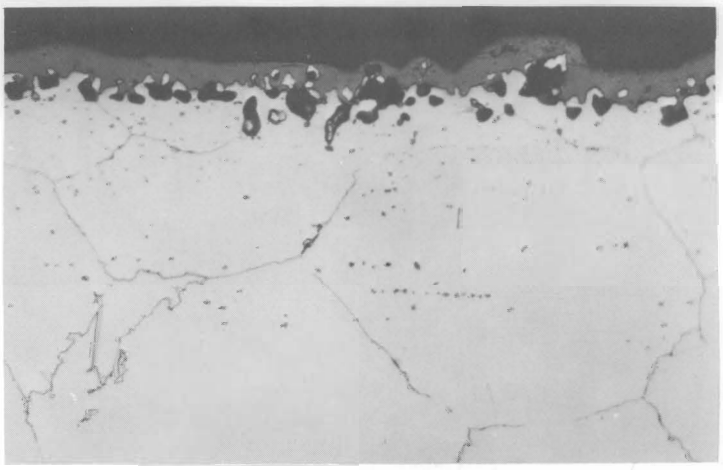

18 μ oxygen
84 hr exposure
Etchant: HCl - H_2O_2
4L1832

FIGURE 21

Oxidation of Hastelloy X-280 at 2048 °F

500X

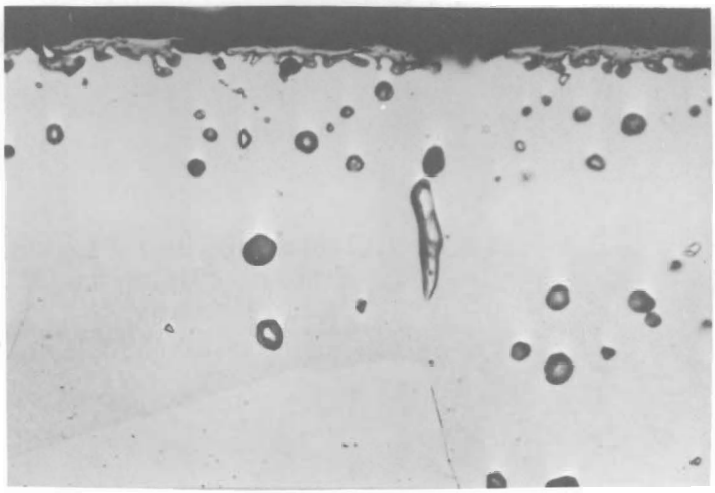

1 atm air
71 hr exposure
Etchant: HCl - H_2O_2
4L1829

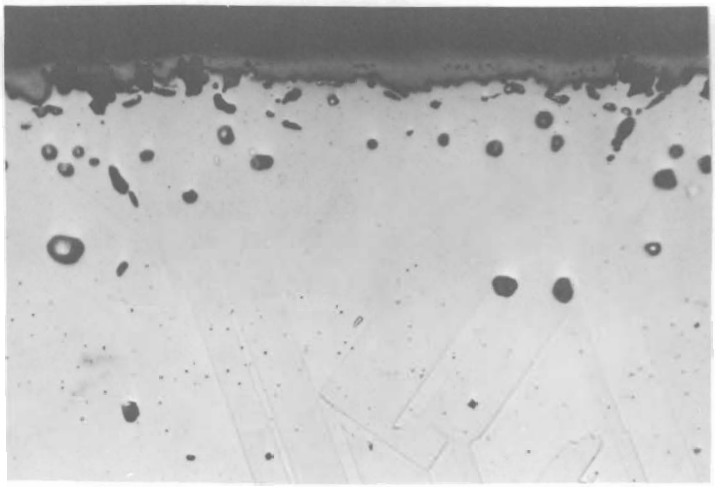

92 μ oxygen
84 hr exposure
Etchant: HCl - H_2O_2
4L1525

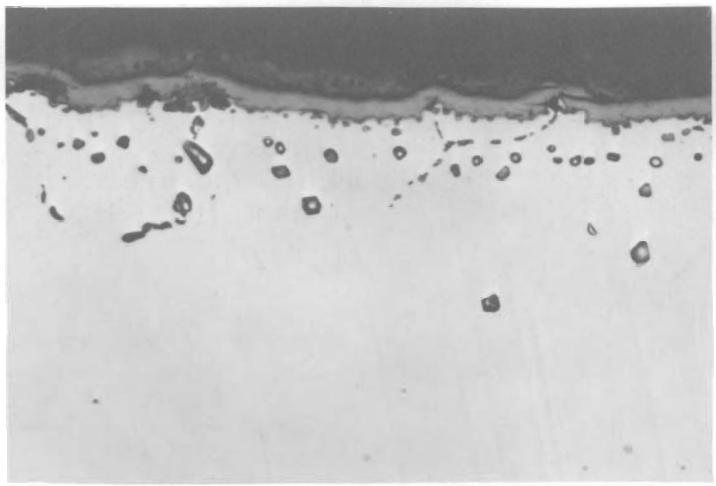

18 μ oxygen
84 hr exposure
Etchant: HCl - H_2O_2
4L1830

FIGURE 22

Oxidation of Haynes Alloy 25 at 2048 °F 500X

Figures 23 and 24 show the weight gain behavior of Hastelloy X-280 at 2192 and 2048 °F, while Figures 25 and 26 show the weight gain behavior of Haynes Alloy 25 at 2192 and 2048 °F in carbon oxides and water vapor. Also included on Figures 23 and 25 is the oxidation of these alloys in oxygen. It is apparent that oxidation proceeds at a lower rate in carbon oxides and in water vapor than in air or oxygen (see also Figures 5 through 8). This is reasonable from a thermodynamic basis because of the relatively low oxygen partial pressures maintained by the respective equilibrium reactions (Appendix I).

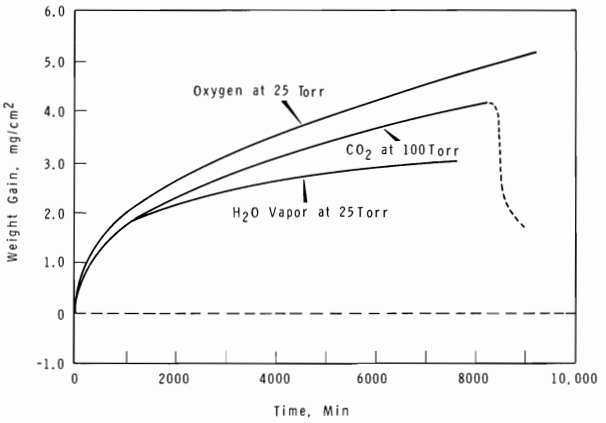

FIGURE 23

Behavior of Hastelloy X-280 at 2192 °F (1200 °C) in Oxygen, Carbon Dioxide, and Water Vapor

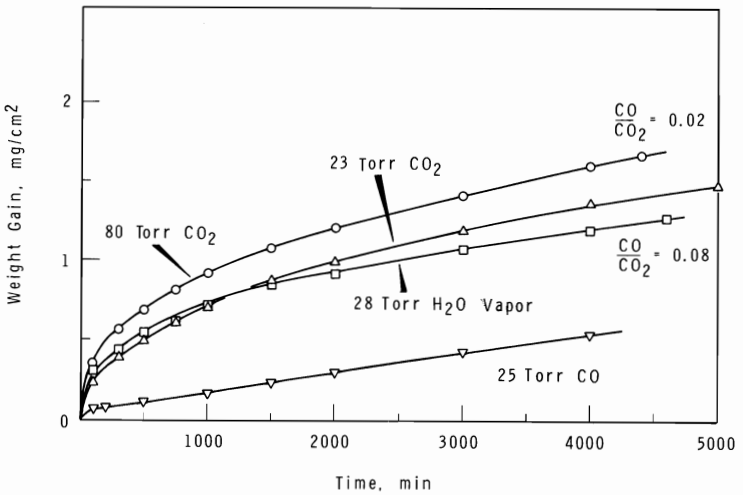

FIGURE 24

Oxidation of Hastelloy X-280 in Carbon Oxides and Water Vapor at 2048 °F (1120 °C)

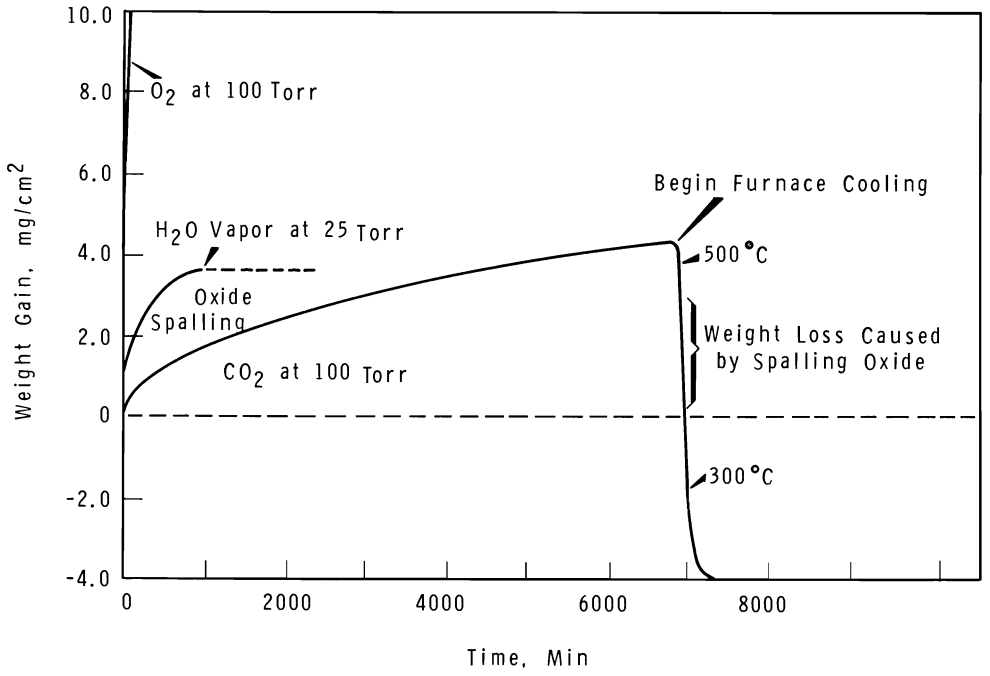

FIGURE 25

Behavior of Haynes 25 at 2192 °F (1200 °C) in Oxygen, Carbon Dioxide, and Water Vapor

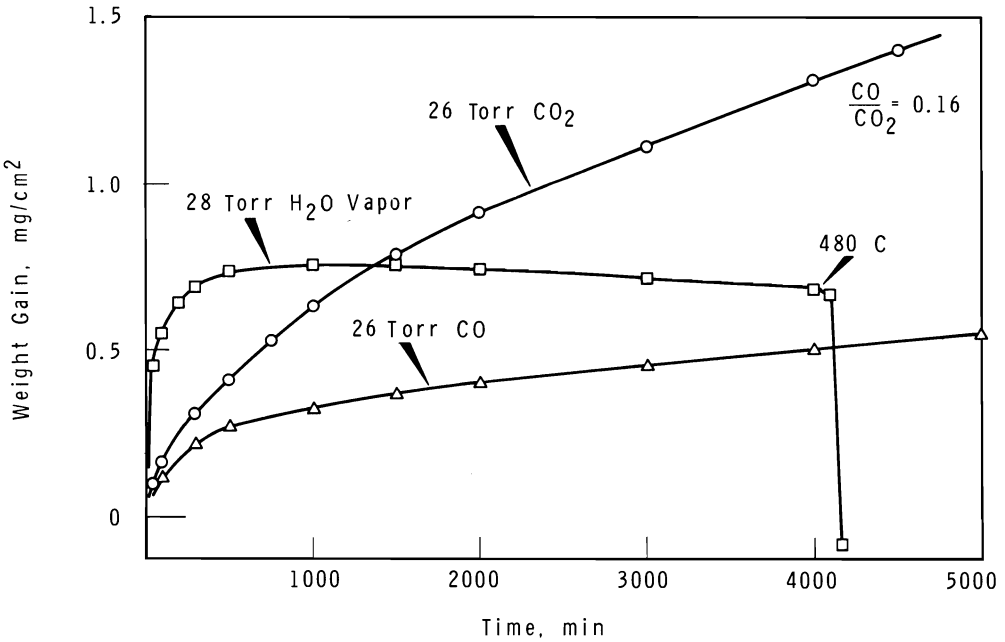

FIGURE 26

Oxidation of Haynes 25 in Carbon Oxides and Water Vapor at 2048 °F (1120 °C)

The oxidizing effect of water vapor at the pressures and temperatures studied is apparent from the weight gain curves. However, the oxidation of Haynes Alloy 25 by water vapor appears to be inhibited after a short time while the oxidation of Hastelloy X-280 does not. The test made on Haynes Alloy 25 at 2192 ^{o}F looked as if spalling was occurring during the oxidation. At 2048 ^{o}F the data obtained was similar to the 2192 ^{o}F run; however, the lack of obvious spalling demanded other reasons for the appearance of the curves. Because the balance-furnace chamber system is unrefreshed, water vapor atmospheres will become contaminated with reaction products (i. e., $H_2O_{(gas)} + Me \rightarrow MeO + H_{2(gas)}$). The formation of hydrogen in this case may tend to reduce the thermodynamic driving force for the corrosion reactions. A reason for the inhibition of Haynes Alloy 25 oxidation may be due to the formation of oxides which are less stable at lower hydrogen concentrations, i. e., more easily reduced by hydrogen than the oxides formed on Hastelloy X-280 (Appendix I lists the water to hydrogen ratios for dissociation of several metal oxides).

In carbon dioxide atmospheres, the corrosion product will be carbon monoxide. Since carbon monoxide can act as either a reducing or oxidizing atmosphere at these temperatures, depending upon the metal involved, it should not be expected that any marked inhibition in reaction rate would be apparent for either superalloy. The curves presented bear this out.

To determine the extent of corrosion on these alloys by pure carbon monoxide, weight gain tests were conducted and are shown in Figures 24 and 26. Osthagen [14] has considered the oxidation of an 80 Ni-20 Cr alloy over a temperature range of 750 to 1000 ^{o}C in carbon monoxide atmospheres. From a thermodynamic basis, the most probable reaction was shown to be

$$3\,[Ni_mCr_{(n+1)}] + CO \rightleftarrows 3\,[Ni_mCr_n] + 1/3\ Cr_2O_3 + 1/3\ Cr_7C_3$$

which at 1000 ^{o}C gave a critical carbon monoxide pressure of 9 Torr. Above this pressure the alloy oxidizes to the indicated products; below this pressure there was a weight loss of the alloy due to metal evaporation. An extrapolation of Osthagen's pressure-temperature data to 1100 ^{o}C gives a critical carbon monoxide pressure of 100 Torr for weight gain.

Applying Osthagen's results to the corrosion data of Hastelloy X-280 and Haynes Alloy 25 (both having approximately 20 wt% Cr) and assuming the thermodynamics of the systems are comparable, oxidation would not be expected to take place at the test pressures in pure carbon monoxide (Figures 24 and 26). A portion of the oxidation (weight gain) shown can be attributed to the slow in-leakage of air through the "impermeable" reaction tube. However, from leak rates through the tube, only about 50% of this weight gain is directly accountable to in-leakage. Therefore, the rest of the weight gain must be due to the oxidation of the alloy by carbon monoxide.

In general, the intensity of attack in each of the gases increases as their respective oxygen partial pressures increase due to dissociation (Appendix I). That is, carbon monoxide will attack Haynes Alloy 25 or Hastelloy X-280 less than water vapor or carbon dioxide at the same relative pressures.

Metallography indicates that the corrodent, whether it is oxygen, water vapor, carbon dioxide, or carbon monoxide, has approximately the same effect on the microstructure (Figures 27, 28, 29, and 30). No intergranular corrosion was observed in any atmosphere. The formation of carbides due to the CO_2 or CO atmospheres were not clearly indicated although Haynes Alloy 25 in 26 Torr CO_2 (Figure 30) shows a microstructure suggesting some carbide formation.

It should be mentioned that the probability of carbide formation in the base metal due to the dissociation reactions of CO_2, CO, or CH_4 decreases sharply if the atmosphere is oxidizing.

Corrosion in a Carburizing Atmosphere

It is conceivable that a situation can exist where the coolant gas stream in the ATR loop can become contaminated with various hydrocarbons. These hydrocarbons could originate from pump oils, greases, etc., which would dissociate at the higher temperatures to carbon, hydrogen, and simpler hydrocarbons. The structural material would then be susceptible to such contamination.

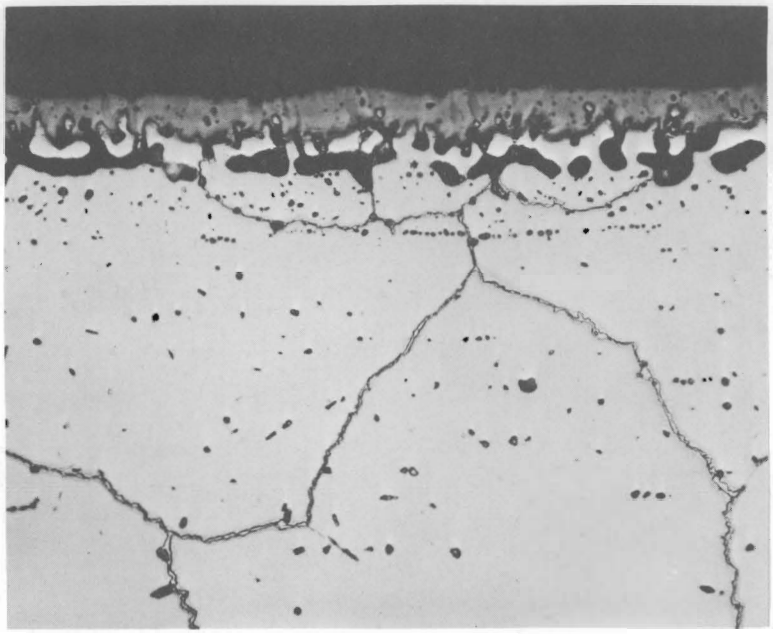

100 Torr carbon dioxide
137 hr exposure
Etchant: HCl - H_2O_2
4L466

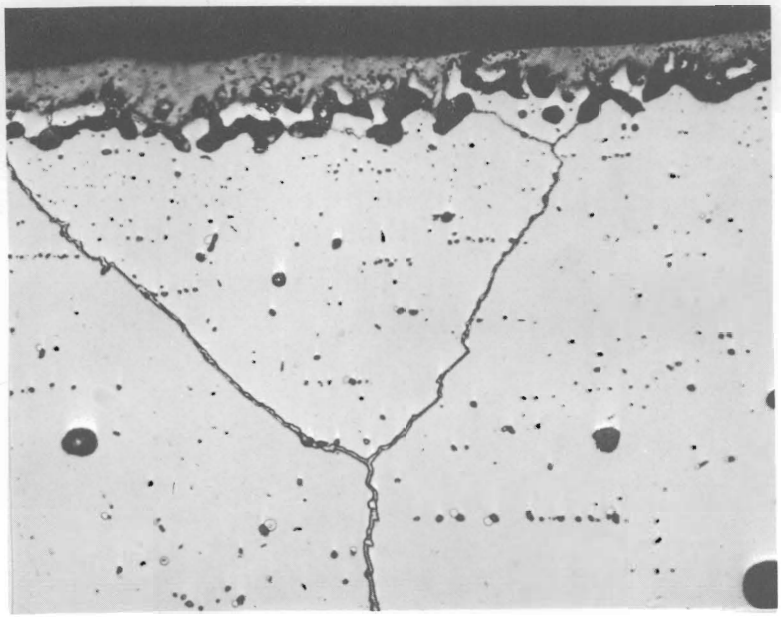

25 Torr Water Vapor
114 hr exposure
Etchant: HCl - H_2O_2
4L468

FIGURE 27
Corrosion of Hastelloy X-280 at 2192 ^{o}F

500X

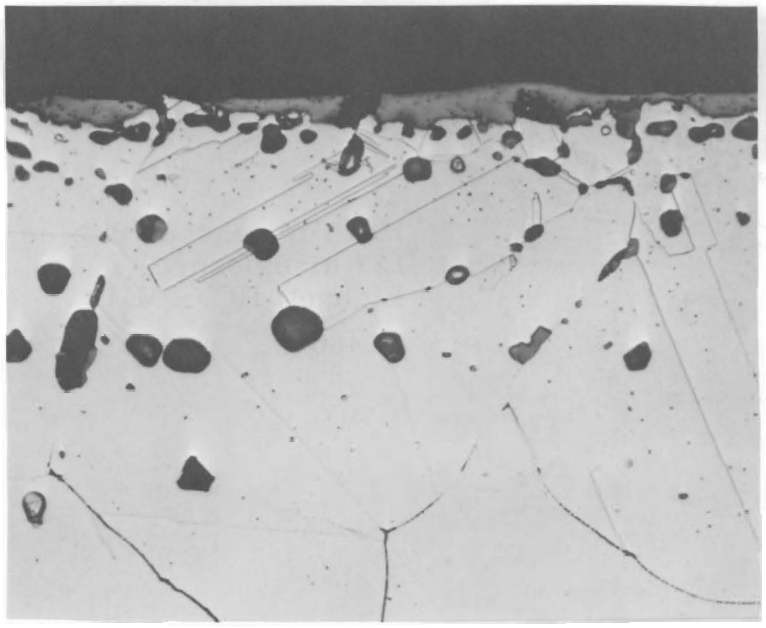

100 Torr carbon dioxide
114 hr exposure
Etchant: HCl - H_2O_2
4L469

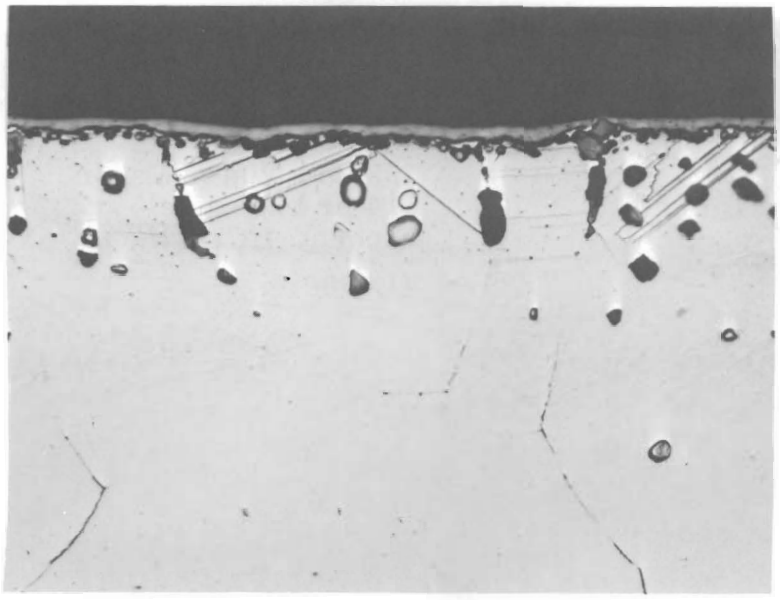

25 Torr water vapor
30 hr exposure
Etchant: HCl - H_2O_2
4L467A

FIGURE 28
Corrosion of Haynes Alloy 25 at 2192 ^{o}F

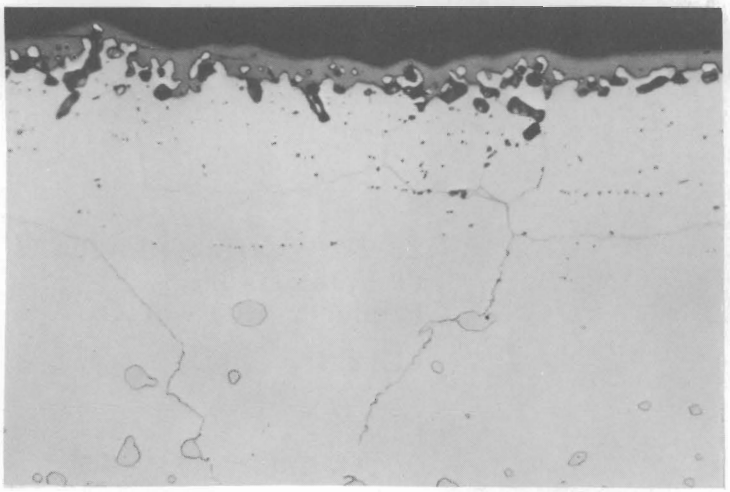

23 Torr carbon dioxide
80 hr exposure
Etchant: HCl - H_2O_2
4L1824

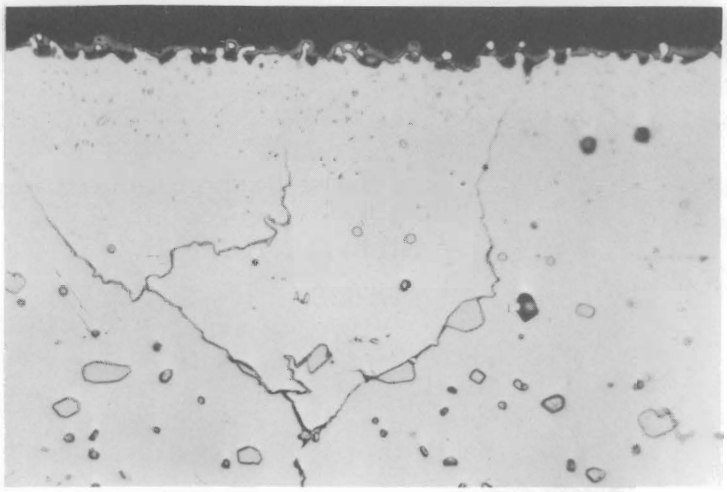

25 Torr carbon monoxide
71 hr exposure
Etchant: HCl - H_2O_2
4L1825

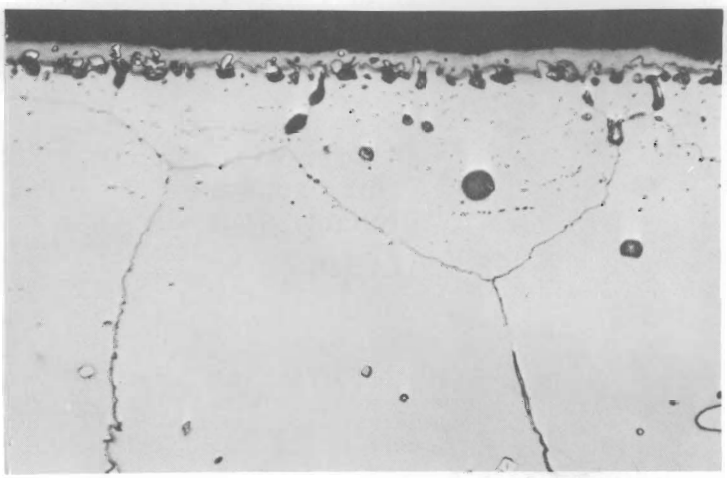

28 Torr water vapor
80 hr exposure
Etchant: HCl - H_2O_2
4L1529

FIGURE 29

Corrosion of Hastelloy X-280 at 2048 ^{o}F

500X

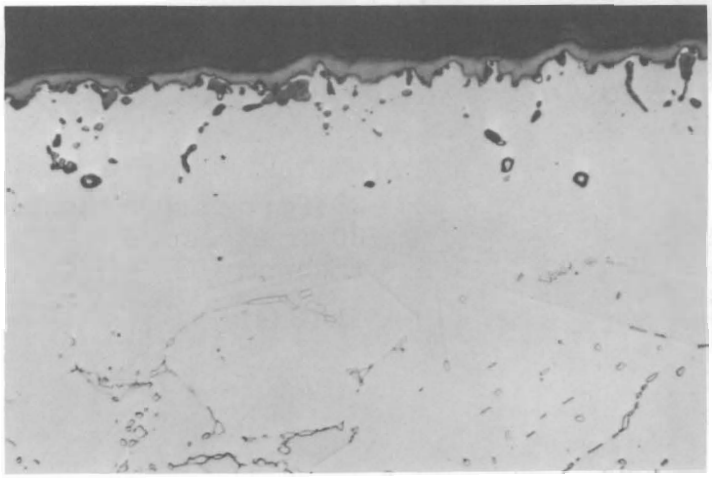

26 Torr carbon dioxide
80 hr exposure
Etchant: HCl - H_2O_2
4L1831

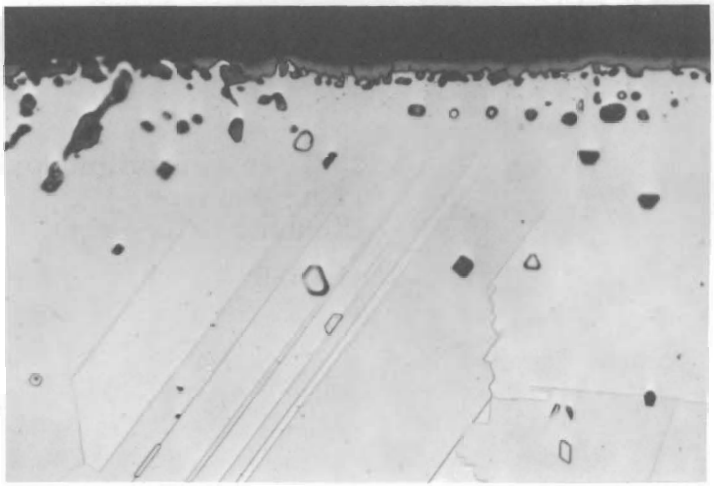

26 Torr carbon monoxide
84 hr exposure
Etchant: HCl - H_2O_2
4L1828

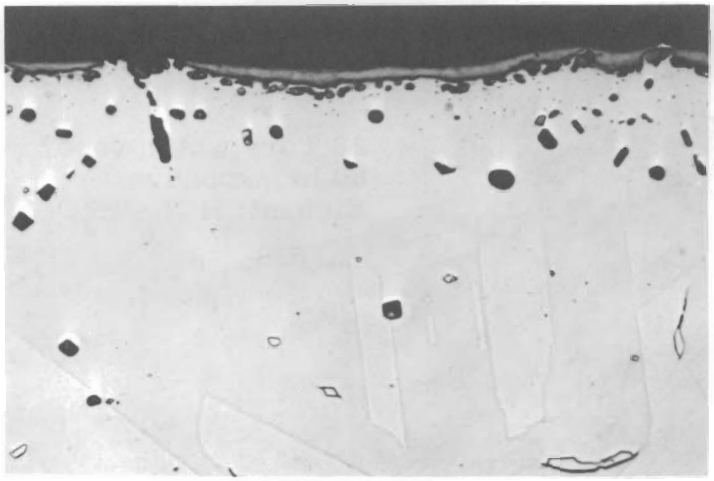

28 Torr water vapor
71 hr exposure
Etchant: HCl - H_2O_2
4L1528

FIGURE 30

Corrosion of Haynes Alloy 25 at 2048 °F

500X

Carburization of Hastelloy X-280 and Haynes Alloy 25 has been carried out in a methane atmosphere at 2048 ^{o}F. The kinetics for the carbon pickup of these alloys taken from weight gain curves (Figure 31) is explained by considering the physical arrangement of the experiment. The slow step for the reaction appears to be the mass transfer of methane from the system reservoirs through the hydrogen reaction product surrounding the sample (gas phase diffusion control). The system reservoir containing the largest amount of methane is the bell jar (Figure 1).

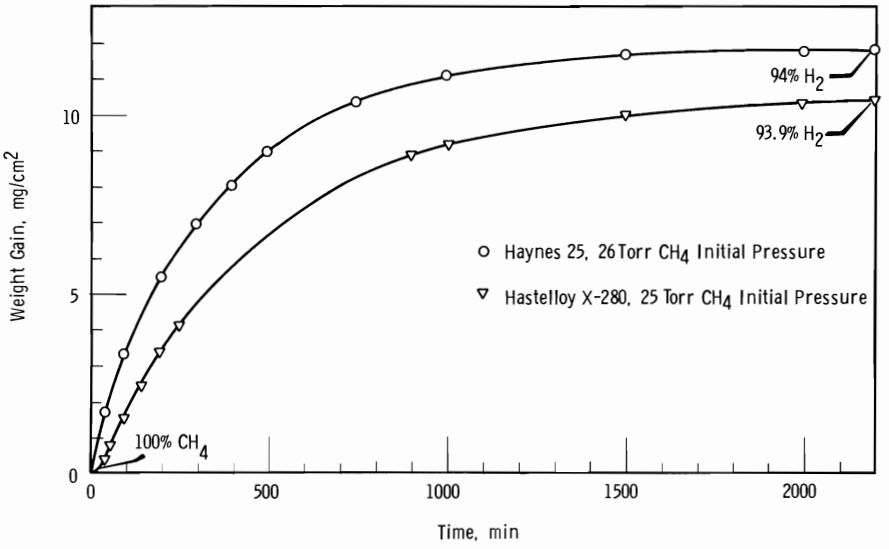

FIGURE 31

Carburization of Hastelloy X-280 and Haynes 25 in Methane at 2048 ^{o}F (1120 ^{o}C)

An equation of the form

$$\ln\left(1 - \frac{\Delta W}{M}\right) = - kt$$

fits the data provided reasonable assumptions are made regarding the initial amount of carbon in the system and the effective diffusion path. The diffusion equation is derived in Appendix III.

Figure 32 shows the extent of carbon pickup by these alloys. X-ray diffraction patterns taken to identify the surface composition did not indicate specific carbides. It appeared that, in the case of Hastelloy X-280, a metal carbide, Cr_7C_3 or $(Cr, Fe)_7C_3$, was present. For Haynes Alloy 25, there were indications of a mixed carbide, M_6C.

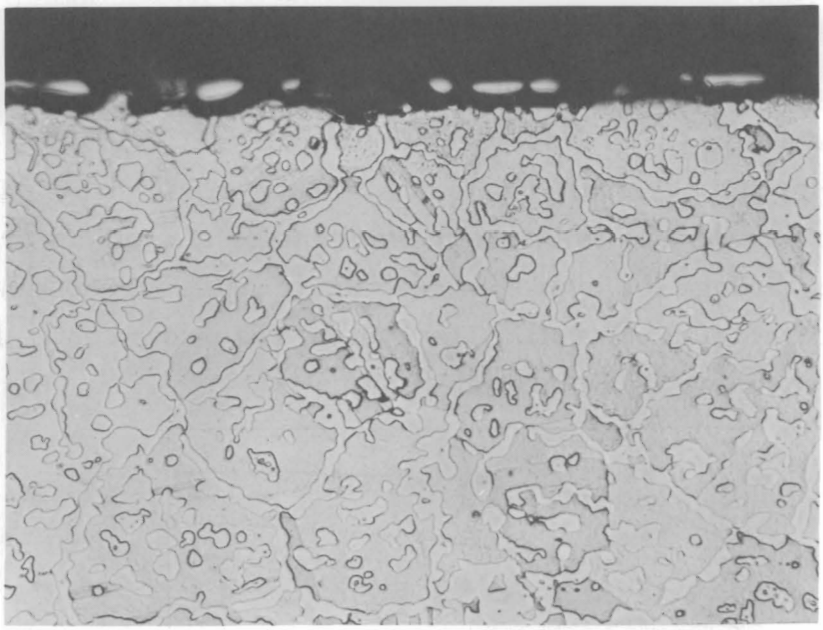

Hastelloy X-280
25 Torr methane
37 hr exposure
Etchant: HCl - H_2O_2
4L1532

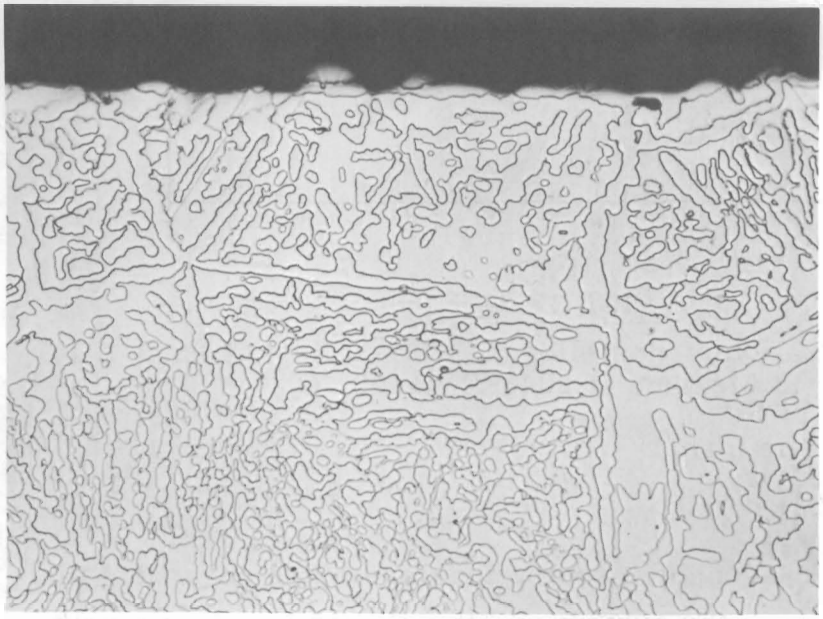

Haynes Alloy 25
26 Torr methane
37 hr exposure
Etchant: HCl - H_2O_2
4L1531

FIGURE 32

Carburization of Hastelloy X-280 and Haynes Alloy 25 in Methane at 2048 °F

500X

From an engineering standpoint, the data illustrate the ease and rapidity of carburization of the superalloys at 2048 °F. The data also show that trace hydrocarbons present in the ATR gas stream could react with the materials of construction as well as with the refractory metal test samples.

The reverse process of carburization, i.e., decarburization, must also be considered. To investigate the decarburization reaction in Hastelloy X-280 and Haynes Alloy 25, coupon samples were carburized in a methane atmosphere and then placed in a 0.1 Torr oxygen replenished atmosphere.

During the first 100 min of the reaction in oxygen, there was a weight loss in both samples corresponding to the weight gained by the coupons during the carburization process (Figure 33). This weight loss is attributed to the removal of carbon from the metal as gaseous carbon oxides. After this initial weight loss, a continual weight gain took place due to the oxidation of the metal. Within experimental limits, the relative rate of oxidation of the carburized coupons compares favorably to the alloys oxidized in the as-received and abraded condition under similar test conditions.

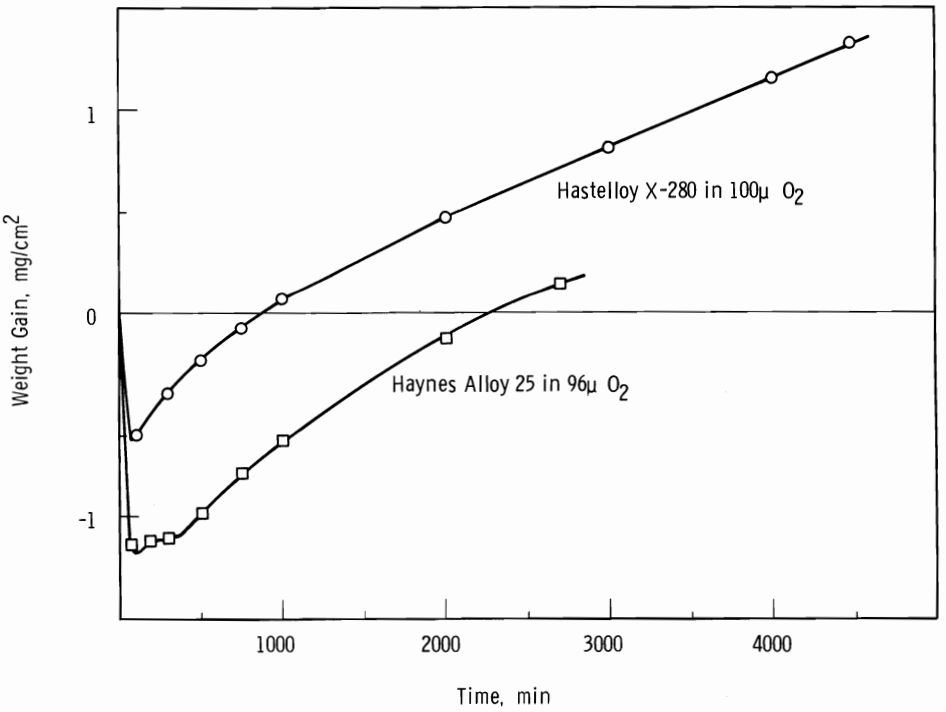

FIGURE 33

Oxidation of Carburized Super Alloys
at 2048 °F in a Replenished Gas System

Figures 34 and 35 show the relative degree of surface carburization of the alloys and the subsequent removal of the carbon and formation of the oxide layer. For both Hastelloy X-280 and Haynes Alloy 25, there appears to be no marked effect on the oxidation resistance due to the carbon removal and subsequent oxidation.

The major effects produced by carbon contamination of the alloys are the loss of ductility and the consequent danger of cracking during deformation. Both the carburized and carburized, then oxidized samples were bent in a U-shape to test the degree of ductility retained in each case. The carburized samples showed little ductility before breaking; the samples permitted a bend of about 45 ^{o} from the longitudinal axis. The carburized, then oxidized samples were bent and smashed flat with no indication of brittleness.

Corrosion in a Nitrogen Atmosphere

The possibility of reactions between nitrogen and superalloy constituents was investigated at 2192 ^{o}F (1200 ^{o}C) by exposing Hastelloy X-280 and Haynes Alloy 25 to nitrogen at 100 Torr pressure for intervals up to 4 days.

During the test period, both alloys lost weight slowly, apparently due to an evaporation mechanism inhibited by the presence of an essentially inert gas overpressure. The weight loss was insignificant, amounting to a maximum penetration of 0.05 mil in the case of Haynes Alloy 25 after 4 days exposure. No unusual nitride phases were noted in the metallography (Figure 36), and the specimen surfaces were relatively smooth. After completion of the test, the samples were bent into a U-shape and smashed flat. No cracking was observed, indicating complete retention of ductility.

The nitride most likely to form in the superalloys at 2192 ^{o}F is $Cr_2N_{0.76}$, which is reported to have a dissociation pressure at 2192 ^{o}F of 6.25 mm.[15] As this pressure is much less than the nitrogen pressure to which the superalloy specimens were exposed, the reason for the lack of nitride formation must lie in the low chemical activity of the chromium present as a solute in the superalloys. This explanation can be rationalized thermodynamically.

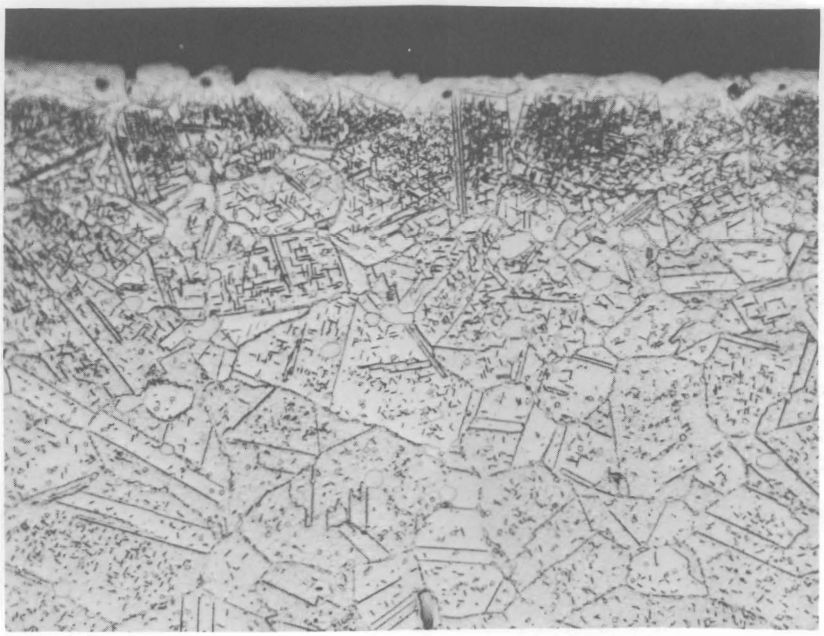

As-carburized at 900 °C
25 Torr methane
12 hr exposure
Etchant: HCl - H_2O_2
4L1883

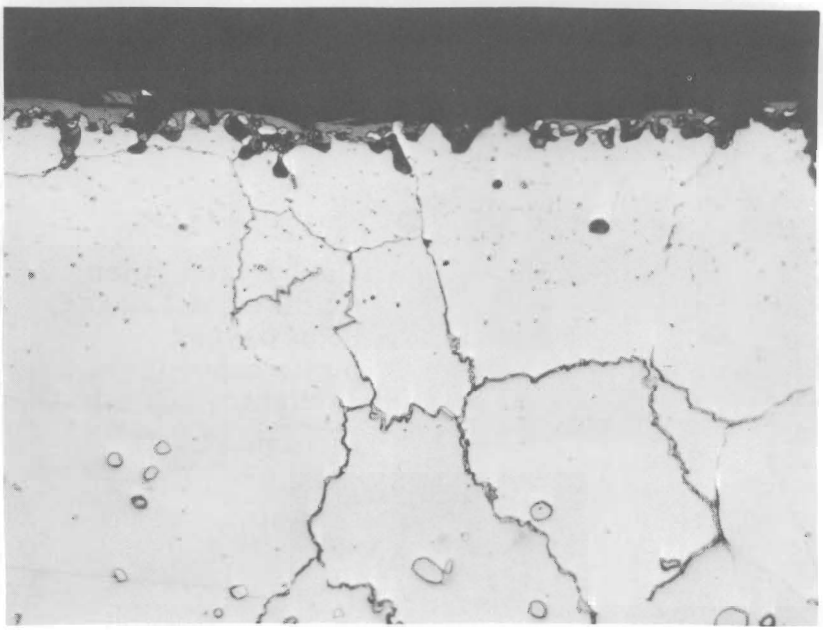

Carburized, then
oxidized at 1120 °C
100 μ oxygen
75 hr exposure
Etchant: HCl - H_2O_2
4L1885

FIGURE 34

Hastelloy X-280: Carburized and Decarburized 500X

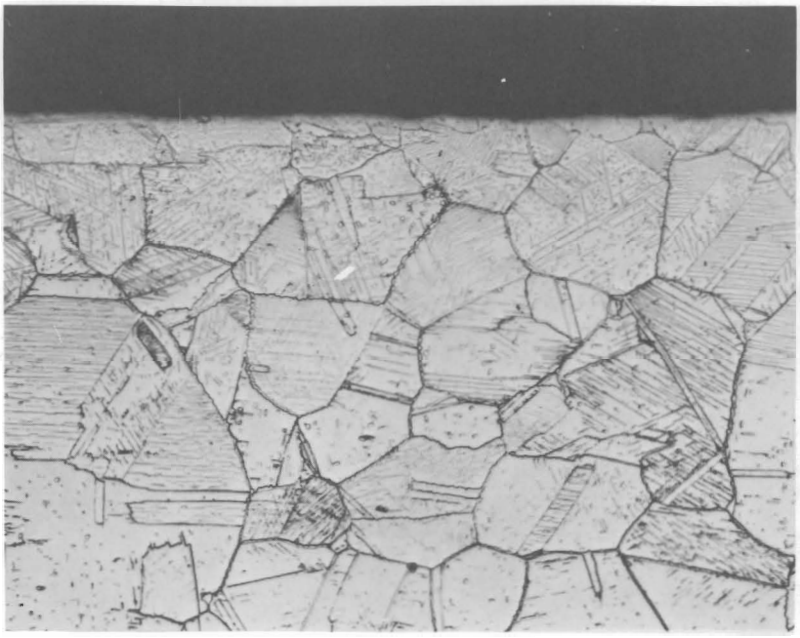

As-carburized at 900 °C
25 Torr methane
12 hr exposure
Etchant: HCl - H_2O_2
4L1887

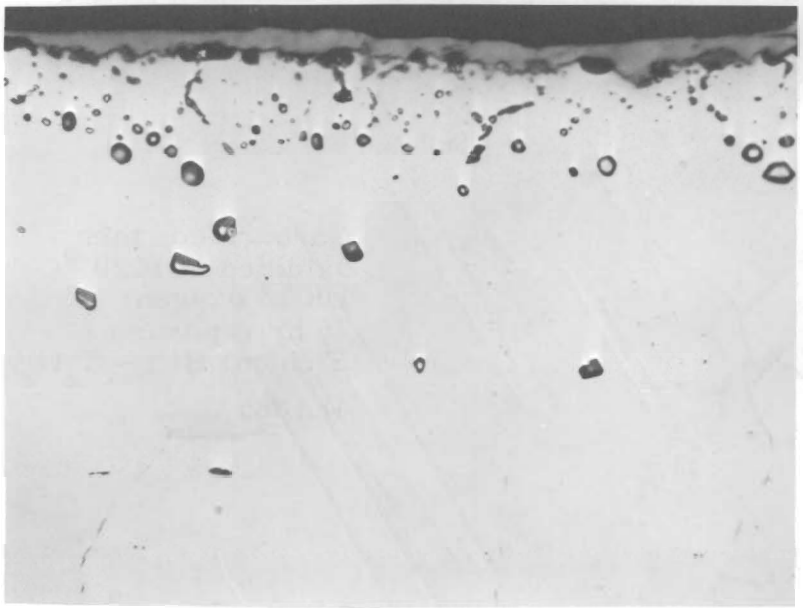

Carburized, then
oxidized at 1120 °C
96 μ oxygen
50 hr exposure
Etchant: HCl - H_2O_2
4L1889

FIGURE 35
Haynes Alloy 25: Carburized and Decarburized 500X

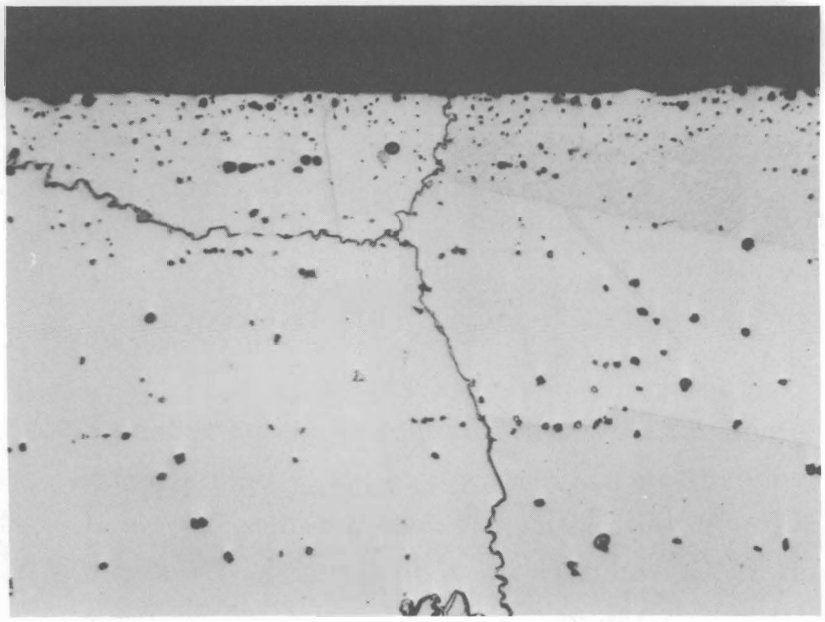

Hastelloy X-280
100 Torr nitrogen
93 hr exposure
Etchant: HCl - H_2O_2
4L67

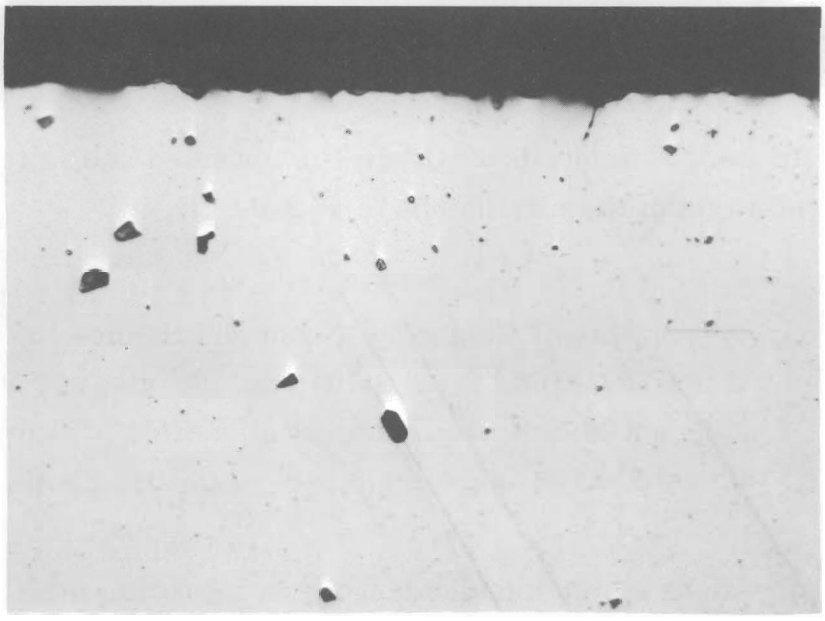

Haynes Alloy 25
100 Torr nitrogen
85 hr exposure
Etchant: HCl - H_2O_2
4L70

FIGURE 36

Hastelloy X-280 and Haynes Alloy 25
After Exposure to Nitrogen Atmosphere at 2192 ^{o}F

500X

The equilibrium constant for the nitriding reaction may be written

$$K = \frac{(A_{Cr})^2 \cdot (P_{N_2})^{0.38}}{A_{Cr_2N_{0.76}}}$$

If we take the activity of chromium saturated with nitrogen (A_{Cr}) and the activity of the pure nitride ($A_{Cr_2N_{0.76}}$) to be equal to unity (good assumptions), and if the pressure of nitrogen (P_{N_2}) is expressed in mm Hg, then K = 2.0 at 2192 °F (1473 °K).

If the chromium is now dissolved in a nickel- or cobalt-base alloy, its chemical activity is reduced to a value which can only be estimated due to lack of relevant data. If the solution is assumed to be ideal, the activity of the chromium is equal to its mol fraction, or about 0.2 for both Hastelloy X and Haynes Alloy 25. Substitution in the foregoing equation yields

$$2.0 = \frac{(0.2)^2 \cdot (P_{N_2})^{0.38}}{(1)}$$

Solving for P_{N_2}, a value of 3×10^4 mm (about 40 atm) is obtained and is the nitrogen pressure required to form the nitride phase at 2192 °F.

Evaporation

The evaporation characteristics of Hastelloy X-280 and Haynes Alloy 25 were determined at 2192 °F, 2105 °F, and 2048 °F; Inconel 600 was studied at 2192 °F only. The weight losses occurring as a function of time are plotted in Figures 37, 38, and 39. All specimens were abraded on 400X emery prior to testing.

The surfaces of specimens which have undergone evaporation are shown in Figures 40 and 41. The nonuniform surfaces formed in the case of Haynes Alloy 25 and Hastelloy X-280 and the large voids formed beneath the surface in all cases can be seen in these figures.

The selective volatilization of alloy constituents (probably primarily chromium) is believed to cause the voids. The convolute surface formed on Hastelloy X-280 after only a 10 hr exposure at 2192 ^{o}F is graphic evidence that the evaporation mechanism does not lead to a uniform attack of this alloy and that the assumption of uniform attack is optimistic. The surface formed in vacuo resembles the metal underneath the oxide film which was formed in air after 78 hr exposure at 2192 ^{o}F (Figure 40). Wlodek [6] concludes that diffusion of Cr^{+3} (outward) through $NiO\text{-}Cr_2O_3$ is the rate controlling step in the thick film oxidation of Hastelloy X. Since a similar mechanism is thought to be operative in the case of evaporative losses, it is not surprising that the metal surface should possess similar diffusion-formed characteristics in either case. In the case of evaporation, less volatile components (such as Mo and W, perhaps in carbide form) have apparently been concentrated at the outer surface as a separate phase with protective characteristics. A separate surface phase also exists in the case of evaporation of Haynes Alloy 25. Inconel 600 shows a relatively smooth surface after volatilization, but large voids exist below the surface of the metal.

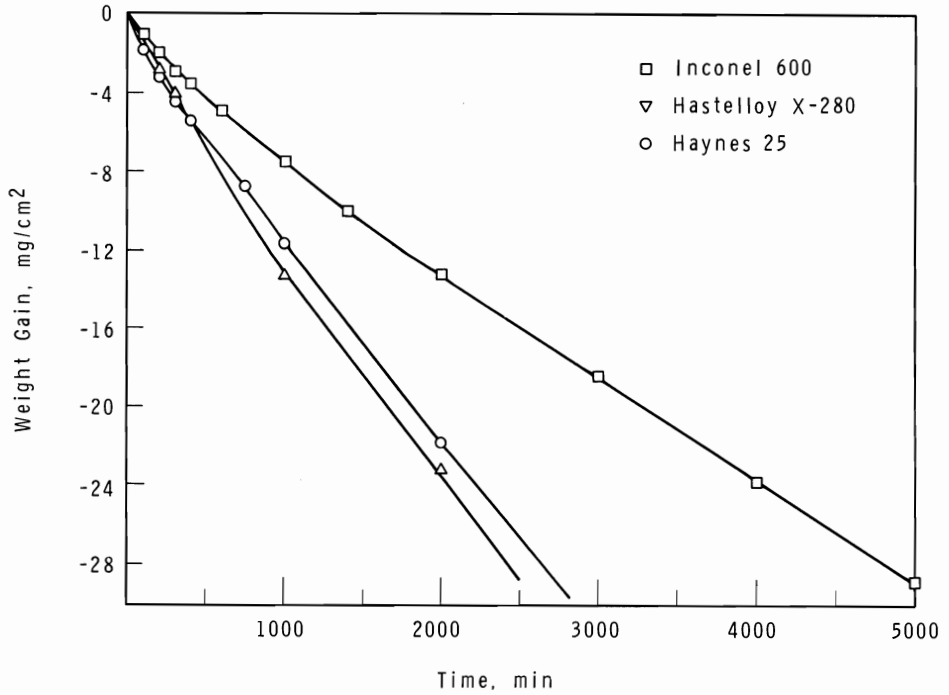

FIGURE 37

Evaporation of Hastelloy X-280, Inconel 600 and Haynes 25 at 2192 ^{o}F (1200 ^{o}C)

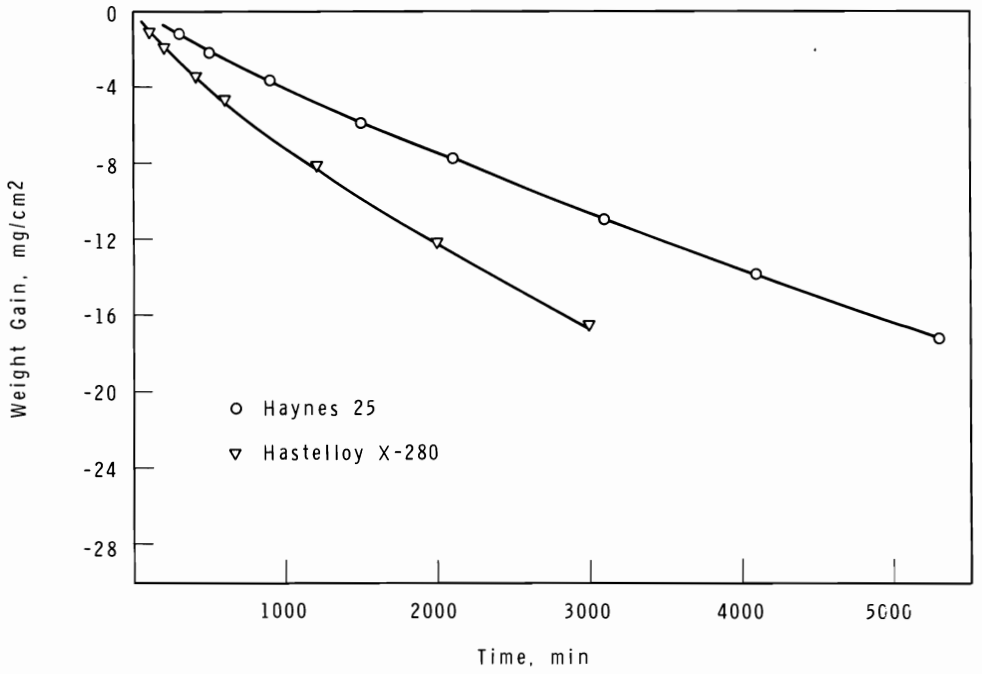

FIGURE 38

Evaporation of Hastelloy X-280 and Haynes 25 at 2102 ^{o}F (1150 ^{o}C)

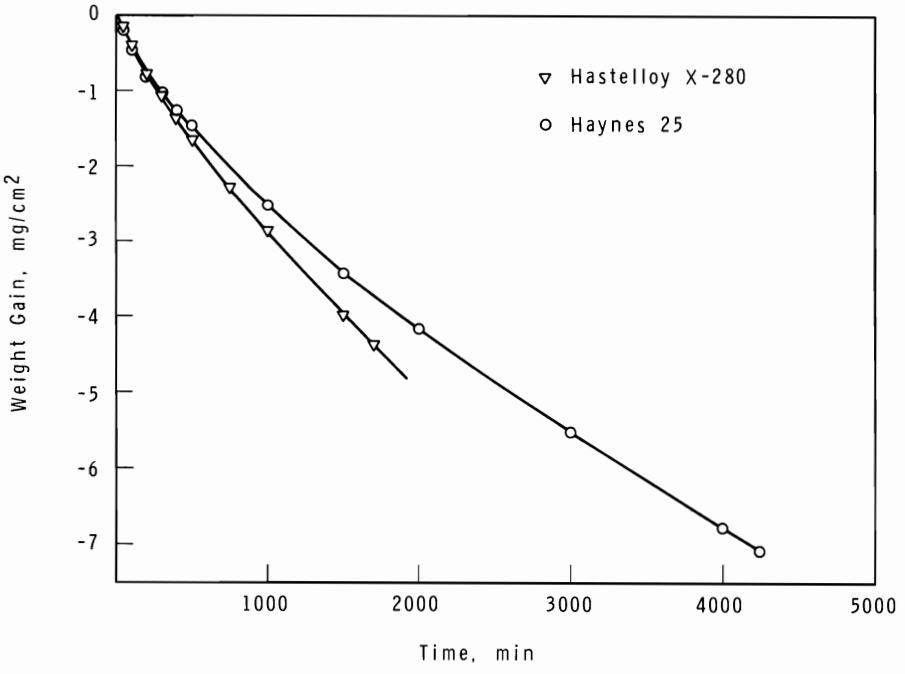

FIGURE 39

Evaporation of Hastelloy X-280 and Haynes 25 at 2048 ^{o}F (1120 ^{o}C)

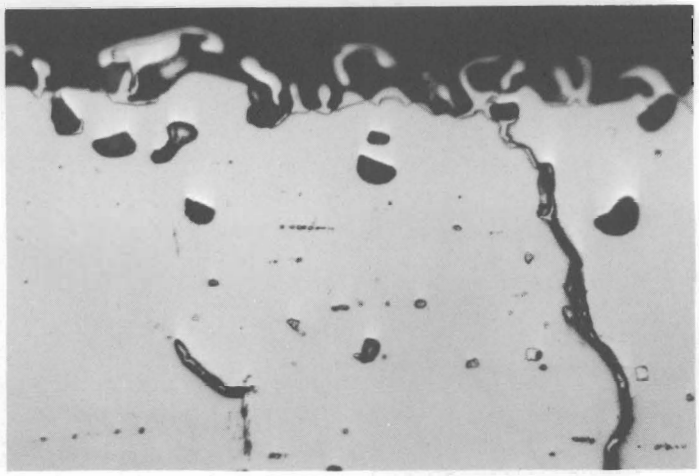

Hastelloy X-280
10 hr exposure
Etchant: HCl - H_2O_2
4L65

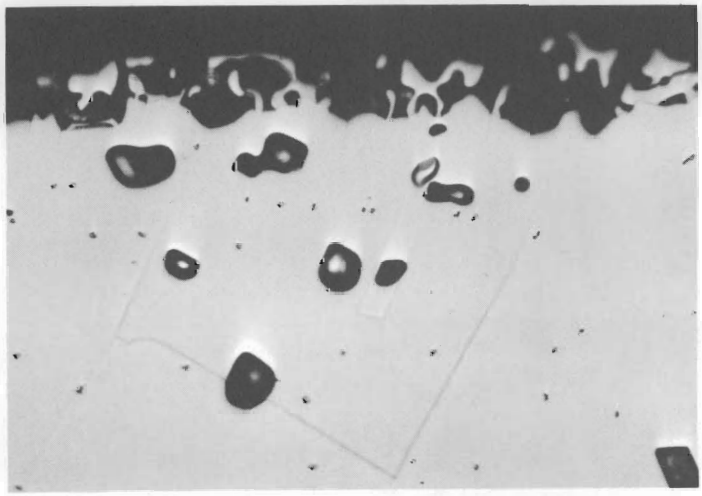

Haynes Alloy 25
55 hr exposure
Etchant: HCl - H_2O_2
4L64

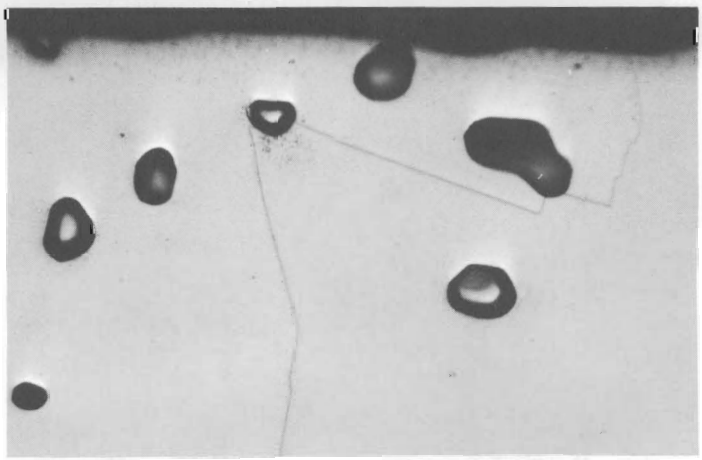

Inconel 600
92 hr exposure
Etchant: 97 HCl - $3HNO_3$ - $5\ H_2SO_4$
4L73

FIGURE 40

The Effect of High Vacuum on Superalloys at 2192 °F

596X

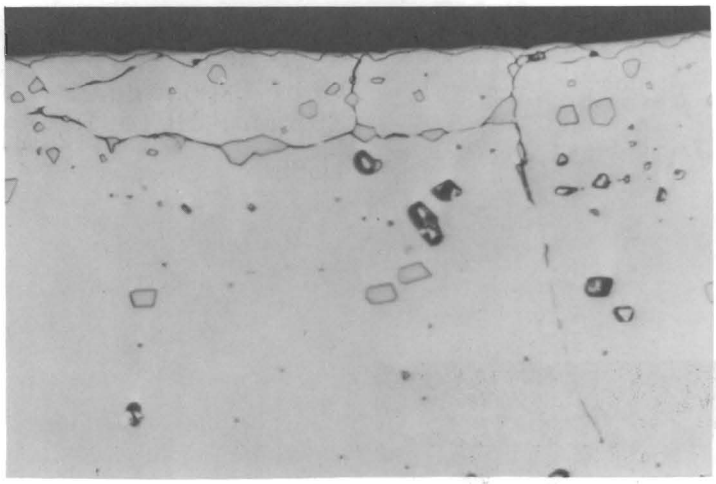

Hastelloy X-280
30 hr exposure
Etchant: HCl - H_2O_2
4L1827

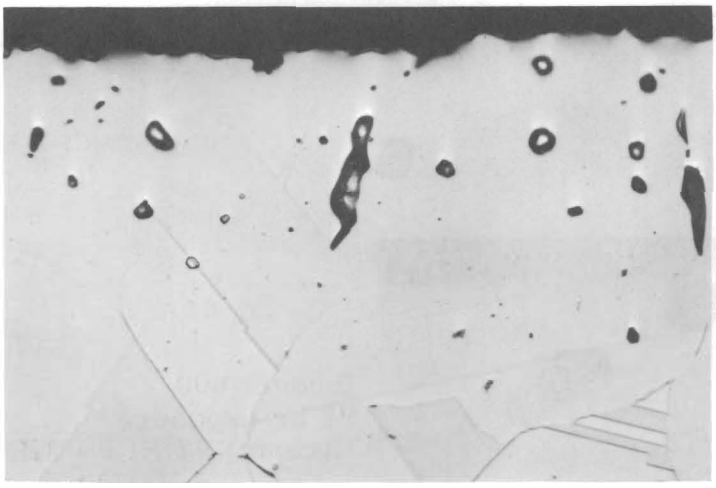

Haynes Alloy 25
71 hr exposure
Etchant: HCl - H_2O_2
4L1826

FIGURE 41

The Effect of High Vacuum on Superalloys at 2048 ^{o}F 500X

From the standpoint of metal loss, it appears that Hastelloy X-280 and Inconel 600 will suffer more damage in vacuum conditions than they will in air at 2192 and 2048 ^{o}F. Haynes Alloy 25 is more stable in vacuum at 2192 ^{o}F than in air (Figure 13). However, at 2048 ^{o}F vacuum damage is more severe for both Haynes Alloy 25 and Hastelloy X-280. The rates of evaporation of the three alloys tested are similar, and all alloys tested show a continual decrease in rate with time. Bates [10] found a linear rate of evaporation after 10 hr exposure at a specified temperature for several alloys. Bates showed that the vapor deposits, produced during evaporation of nickel-base alloys containing chromium, contain both nickel and chromium, even though chromium has a much higher vapor pressure than nickel. For example, after holding Nichrome V (80% Ni–20% Cr) in vacuo at 1150 ^{o}C for 2 hr, a vapor deposit shows 46% Ni and 51% Cr. Bates found an evaporation rate for Hastelloy X about three times as high as that reported in the present work. This can probably be explained by the experimental set-up: Bates' samples were positioned in a tube, open on both ends, in a large bell jar so that metal vapors could escape in both directions. The samples used in the present study were hung in a closed-end furnace tube so that metal vapors could escape in one direction only. The higher resultant metal vapor pressures surrounding the sample could account for the lower evaporation rate.

Metal loss by evaporation can be greatly retarded by formation of a continuous oxide film. Table III indicates metal penetration at three days (4320 min) for several of the conditions and temperatures previously discussed. These penetration data assume uniform evaporation or oxidation with no internal oxidation or alloy depletion. Because of these assumptions, the data indicate less metal degradation than actually occurs and is used only for rough comparative purposes.

At present, evaporation in the ATR loop is not considered to be especially dangerous because the metal surfaces are likely to be covered with a thin layer of oxide, which will reduce metal loss. Erosion effects appear to be the only possible danger from the flowing gas. As yet, this potential danger has not been sufficiently explored.

TABLE III

PENETRATION[(a)] OF HASTELLOY X-280

Temperature	Atmosphere	Weight Gain mg/cm^2 (3 days)	Penetration, mils (3 days)
2048 °F	1 atm air	2.44	0.34
	25 Torr oxygen	2.90	0.41
	3.3 Torr oxygen	2.38	0.33
	97 μ oxygen	2.00	0.28
	39 μ oxygen	1.59	0.22
	18 μ oxygen	1.82	0.25
	10^{-4} Torr vacuum	-4.5 (1750 min)	0.22
2192 °F	1 atm air	3.92	0.55
	25 Torr oxygen	3.60	0.51
	10^{-4} Torr vacuum	-28.8 (2500 min)	1.38
	PENETRATION OF INCONEL 600		
2192 °F	1 atm air	4.7	0.56
	25 Torr oxygen	4.0 (1100 min)	0.48
	5 Torr oxygen	3.6	0.43
	10^{-4} Torr vacuum	-25.5	1.17
	PENETRATION OF HAYNES ALLOY 25		
2048 °F	1 atm air	2.32	0.35
	100 Torr oxygen	3.72	0.56
	25 Torr oxygen	2.08	0.31
	92 μ oxygen	2.35	0.35
	42 μ oxygen	1.52	0.23
	10^{-4} Torr vacuum	-7.15	0.31
2192 °F	1 atm air	18.0 (400 min)	2.70
	100 Torr oxygen	19.0 (600 min)	2.85
	10^{-4} Torr vacuum	-26.6 (2500 min)	1.14

(a) Conversion factors for weight gain to metal penetration listed in Appendix II.

Weldment Corrosion

Weldments tested were Hastelloy X-280 and Hastelloy X-280 (Hastelloy X-280 filler wire), Haynes Alloy-25 and Haynes Alloy-25 (Haynes 25 filler wire), and Hastelloy X-280 and Haynes Alloy 25 (Hastelloy W filler wire).

The samples were loaded in a high temperature tube furnace and exposed to flowing contaminated helium (He + 0.5% O_2 + 0.54% N_2) at 2192 ^{o}F (1200 ^{o}C) for 7 days. Gas flow was maintained at 0.5 scfh.

The condition of the samples at the end of the test period is shown in Figure 42. The Hastelloy X-280–Hastelloy X-280 weldments (Samples 3, 6, and 9) maintained good metallic integrity and were coated with a thin, tenacious film of oxide. The attack on Haynes Alloy 25 increased in severity with downstream position, e.g., Sample 8 is almost completely consumed while Sample 2, located further upstream, is only heavily oxidized. Sample 5 shows intermediate effects. In the case of Hastelloy X-280–Haynes Alloy 25 weldments, the sample position is again important. Upstream Samples 1 and 4 show heavy oxidation with some increased attack on the weld zone. Samples 7 and 10, however, show complete separation of the Haynes Alloy 25 from the Hastelloy X-280 with the Haynes Alloy 25 completely consumed. The weld zone shows oxidation characteristics approximately intermediate between Haynes Alloy 25 and Hastelloy X.

The test proved so severe that only rough qualitative observations can be made. The reason for the more rapid attack on Haynes 25 in the further downstream positions is not known. The oxidation resistance of Haynes Alloy 25 will dictate the oxidation resistance of a Hastelloy X-280–Haynes Alloy 25 couple. The weld zone of the Hastelloy X-280–Hastelloy X-280 couple appeared as oxidation resistant as the parent metal. The sample support constructed of Hastelloy X-280 sheet stock was coated with a thin, hard layer of oxide; it demonstrated good strength and good resistance to the corrosive environment.

Corrosion in Grade A Helium

Two tests were performed to illustrate the corrosive effects of flowing Grade A helium on superalloys at 1900 ^{o}F. In the first test, Grade A

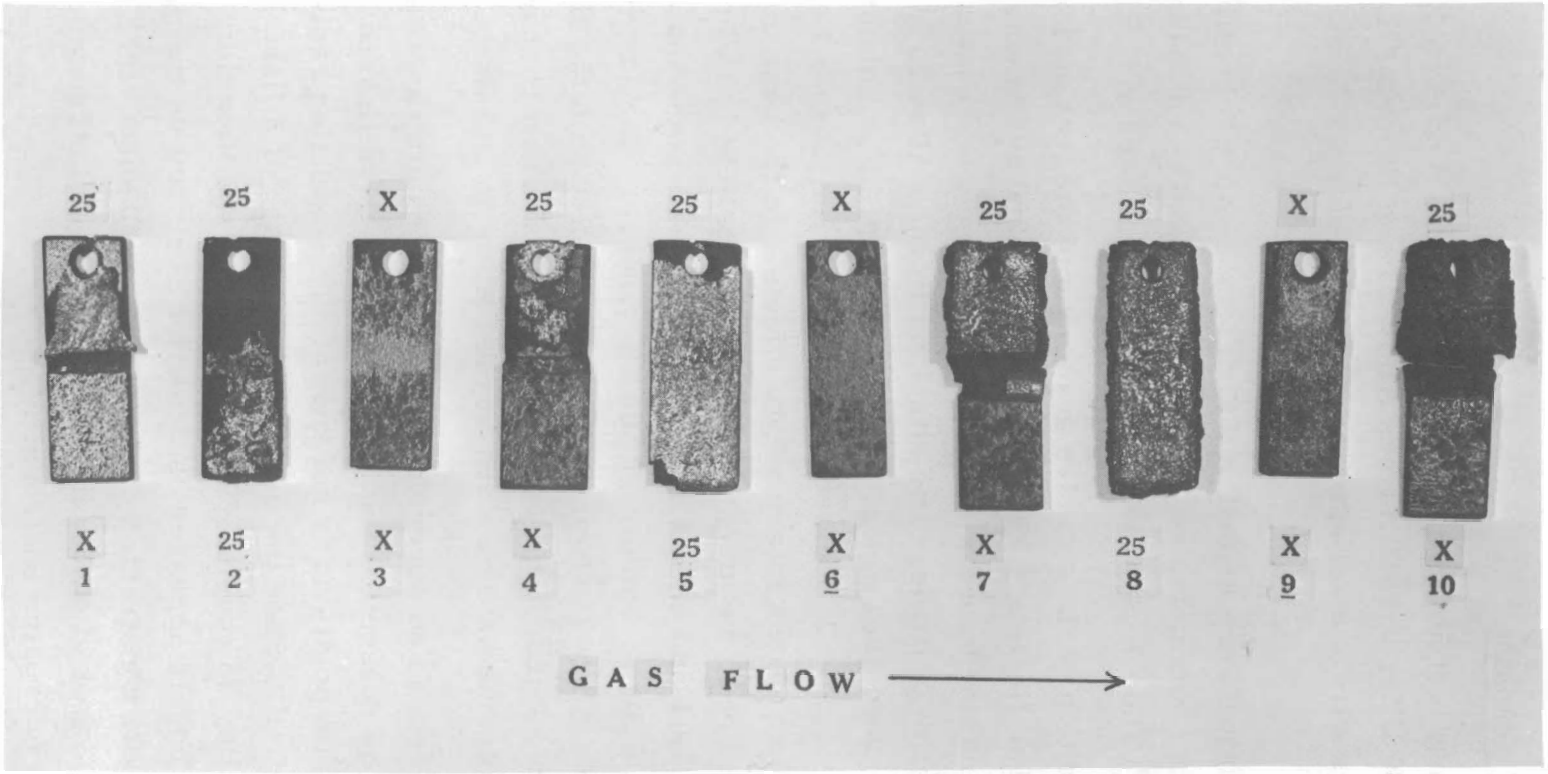

FIGURE 42

Corrosion of Hastelloy X-280 and Haynes Alloy 25 Weldments
in Contaminated Helium at 2192 °F
(Symbol X refers to Hastelloy X; "25" to Haynes 25)

helium of 99.97% analyzed purity was passed over a row of Haynes Alloy 25 samples at a linear flow rate of about 2 in./sec for 10 days, a sufficient time to almost exhaust a standard 1A bottle of helium (220 ft^3, STP). In the second test, the samples were Hastelloy X-280, and an identical test was conducted.

Weight change data for the alloy samples is given in Figure 43, and metallography of the upstream samples is shown in Figure 44. All samples showed a tendency to slough oxide; the Haynes Alloy 25 lead samples were especially bad in this regard. Because of this tendency, the weight change data is not quantitatively meaningful. Also, the helium used in each test came from a different source, a factor which could strongly influence the weight gain results. The "gettering" effect of the upstream samples in both cases is noteworthy and illustrates the difficulties of obtaining consistent weight gain data from sample arrays at low corrodant partial pressures. The metallography shows the superior resistance of Hastelloy X-280 to internal attack under the test conditions.

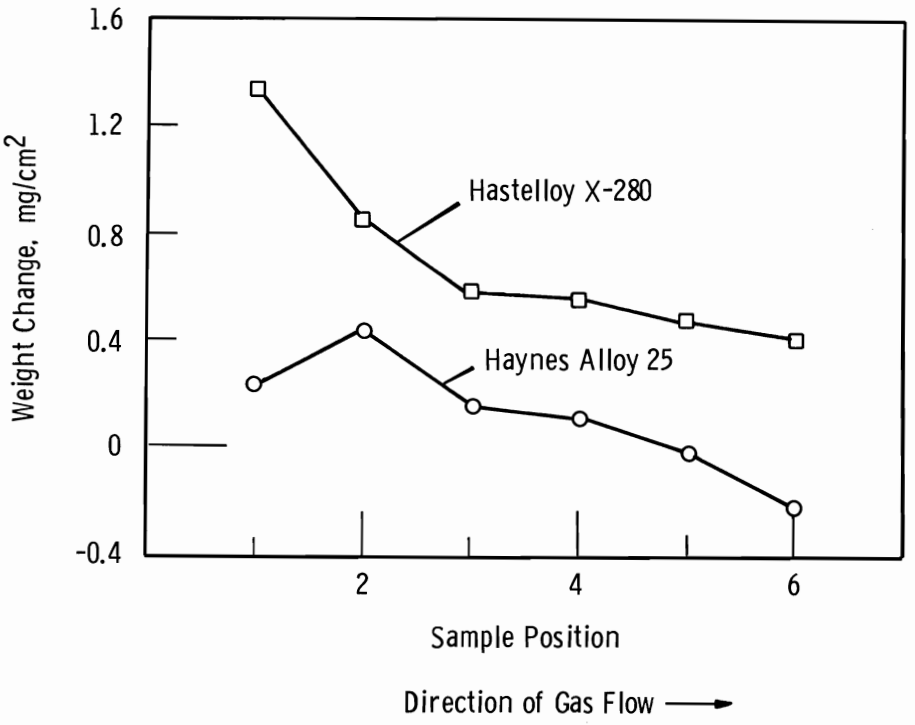

FIGURE 43

Weight Change of Superalloys in Flowing Helium at 1900 °F (1038 °C)

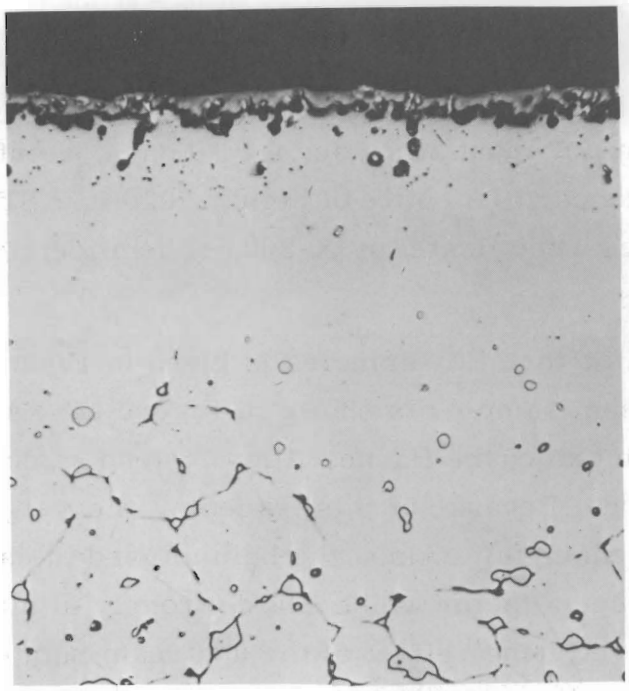

Hastelloy X-280
10 days Exposure
Etchant: HCl - H_2O_2
4K 816

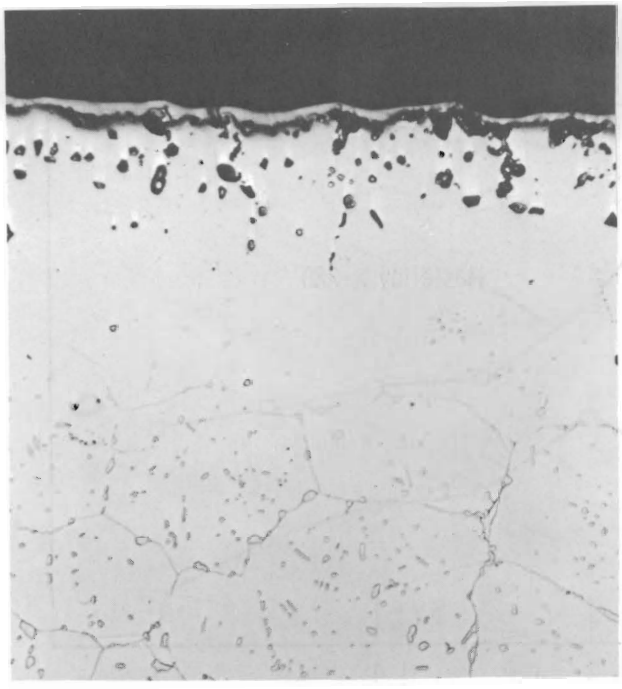

Haynes Alloy 25
10 days Exposure
Etchant: HCl - H_2O_2
4K 814

FIGURE 44

Corrosion of Hastelloy X-280 and Haynes Alloy 25 in Grade A Helium at 1900 ^{o}F 500X

SUMMARY AND CONCLUSIONS

The corrosion data presented in this report was not accompanied by mechanical tests so that the effect of oxidation on the physical properties of the materials tested is not precisely known. Penetration data as given in Table III are optimistic because the metal lost was assumed to be uniformly removed from the sample surface and because internal oxidation and alloy depletion were disregarded. The weight change curves from which the penetration data were obtained cannot be used on a design basis, as other investigators have emphasized the importance of internal attack. Simenz [5] found that Hastelloy X was "affected" to a depth of 1.8 mils after 10 hours exposure at 2200 °F in air. Wlodek [6] found internal oxidation to a depth of about 0.7 mil and alloy depletion to a depth of about 4 mils under approximately the same conditions. Assuming metal loss due to uniform oxidation only, a penetration value of 0.34 mil was found for Hastelloy X-280 in air at 2048 °F after a 3 day exposure. It would appear reasonable to multiply the penetration due to oxidation in air by a factor of five for design criteria. For the case of evaporation, it appears that applying a factor of two to the data would give usable penetration information which should take into account the nonuniformity of the evaporation attack. It has already been mentioned that significant penetration by evaporation is not expected in the ATR loop because of the expected presence of an oxide film on the metal surfaces.

Vacuum data, unfortunately, are not directly applicable to the ATR loop in which high pressure, high velocity helium will be influencing metal degradation.

Because of the complex nature of superalloy oxidation as a function of oxygen pressure and the system dependent nature of the evaporation phenomenon, it is of utmost importance that a careful ATR structural material surveillance program be maintained. Samples which can be withdrawn and analyzed should be located within the loop in positions which offer the most favorable conditions for oxidation and evaporation. In the final analysis, the exact degradation rates of structural materials must be obtained from the ATR gas loop itself.

FUTURE WORK

This document completes the initial survey of gas-superalloy reactions which are probable in the ATR gas loop. It should again be strongly emphasized that the results obtained from a static system containing much higher contaminant gas concentrations per unit metal weight than is expected in the ATR loop can be used only as a guide to potential problem areas and maximum corrosion. Other than for special problems lending themselves to static microbalance work, future testing will be done primarily in the Dynamic Materials Testing Apparatus (DMTA). The results of these tests, which will more closely approximate ATR conditions along with the data presented in this report, should indicate the nature and extent of corrosion which might be expected in the ATR loop.[12, 13]

ACKNOWLEDGMENTS

The authors would like to acknowledge the assistance of R. L. Dillon, who through discussions and review contributed to this report. Personnel of L. A. Hartcorn's Metallographic Laboratory performed the metallography.

APPENDIX I

THERMODYNAMICS OF GAS-METAL REACTIONS

The expected oxygen partial pressure and carbon concentration from the dissociation of pure gases are generally an indication as to the extent or likeihood of a corrosion process. Woodley [16] has tabulated free energy changes for several reactions in the temperature range 300 °K to 2000 °K. The following standard free energy values for four reactions were used to calculate equilibrium data pertinent to the oxidation tests.

TABLE IV

FREE ENERGY FOR GAS DISSOCIATION

Reaction	ΔF^o in cal/mole 1400 °K	1500 °K
1. $CO_{2(g)} \rightleftharpoons CO_{(g)} + 1/2\ O_{2(g)}$	38, 478	36, 434
2. $CO_{(g)} \rightleftharpoons C^o_{(s)} + 1/2\ O_{2\ (g)}$	56, 185	58, 238
3. $CO_{(g)} + H_2O_{(g)} \rightleftharpoons CO_{2(g)} + H_{2(g)}$	2, 179	2, 858
4.[a] $H_2O_{(g)} \rightleftharpoons H_{2(g)} + 1/2\ O_{2(g)}$	40, 557	39, 292

(a) Free energy calculated from (3) and (1)

Considering the dissociation of a pure gas, the free energy at the test temperature can be used to approximate the partial pressures of the dissociation products. As an example, the dissociation of water vapor can be written

$$H_2O(g) \rightleftharpoons H_{2(g)} + 1/2\ O_{2(g)} \qquad (1)$$

The equilibrium constant can then be expressed as

$$K = \frac{\left(P_{H_2}\right)\left(P_{O_2}\right)^{1/2}}{P_{H_2O}} \qquad (2)$$

where P_i is the partial pressure of each gas in atmospheres.

At 1400 ^{o}K (2060 ^{o}F), ΔF = 40,557 cal/mole for (1). By definition

$$K = \exp(-\Delta F/RT) \tag{4}$$

where

R = ideal gas constant, 1.98 cal/(^{o}K)(mole)

T = temperature in degrees Kelvin

or

$$K = \exp[-40,557/(1.98)(1400)] = 4.95 \times 10^{-7}. \tag{5}$$

Letting χ represent the partial pressure of hydrogen, $1/2\ \chi$ will represent the partial pressure of oxygen, and (2) can be written

$$K = \frac{\chi^{3/2}}{P_{H_2O}} \tag{6}$$

For the tests conducted, P_{H_2O} was 28 Torr (0.037 atmospheres).

Substituting the numerical values into (6) and solving for χ,

$$\chi^{3/2} = (0.037)(4.95)(10^{-7}) = 1.72 \times 10^{-8} \tag{7}$$

$$\chi = (1.72 \times 10^{-8})^{2/3} = 6.67 \times 10^{-6} \tag{8}$$

The partial pressure of hydrogen is 6.67×10^{-6} atm (5.07×10^{-3} Torr).

The partial pressure of oxygen is 3.34×10^{-6} atm (2.54×10^{-3} Torr).

The method of calculation for each particular system of interest is the same.

Table V gives the numerical values associated with a particular reaction.

Equilibrium ratios for oxide reduction by hydrogen as well as dissociation pressures for the several metal oxides are listed in Table VI.

TABLE V

DISSOCIATION PRESSURES OF SELECTED GAS REACTIONS

	$H_2O \rightarrow H_2 + 1/2\ O_2$		$CO_2 \rightarrow CO + 1/2\ O_2$		$CO \rightarrow C + 1/2\ O_2$	
	1400 °K	1500 °K	1400 °K	1500 °K	1400 °K	1500 °K
Equilibrium Constant (K)	4.95×10^{-7}	1.98×10^{-6}	1×10^{-6}	5.13×10^{-6}	2.14×10^{-9}	3.39×10^{-9}
Total Initial Pressure (P) Torr	28	28	25	25	25	25
P_{O_2}, Torr	2.54×10^{-3}	1.98×10^{-3}	4.9×10^{-3}	1.46×10^{-2}	3×10^{-18}	2×10^{-17}
P_{H_2}, Torr	5.07×10^{-3}	1.68×10^{-2}	--	--	--	--

TABLE VI

DISSOCIATION PRESSURES FOR METAL OXIDES AND EQUILIBRIUM RATIOS FOR THEIR REDUCTION BY HYDROGEN (17)

	$NiO + H_2 \rightleftarrows Ni + H_2O$	$NiO \rightleftarrows Ni + 1/2\ O_2$
°K	$\frac{H_2O}{H_2}$	P_{O_2} (Torr)
1200	201	4.89×10^{-9}
1400	167	4.31×10^{-6}
1600	142	6.83×10^{-4}

	$CoO + H_2 \rightleftarrows Co + H_2O$	$CoO \rightleftarrows Co + 1/2\ O_2$
°K	$\frac{H_2O}{H_2}$	P_{O_2} (Torr)
1200	32.0	1.35×10^{-10}
1400	27.2	1.15×10^{-7}
1600	24.6	2.05×10^{-5}

	$Cr_2O_3 + 3H_2 \rightleftarrows 2\ Cr + 3H_2O$	$Cr_2O_3 \rightleftarrows 2\ Cr + 3/2\ O_2$
°K	$\frac{H_2O}{H_2}$	P_{O_2} (Torr)
1200	8.77×10^{-5}	9.35×10^{-22}
1400	5.40×10^{-4}	4.53×10^{-17}
1600	2.10×10^{-3}	1.50×10^{-13}

	$FeO + H_2 \rightleftarrows Fe + H_2O$	$FeO \rightleftarrows Fe + 1/2\ O_2$
°K	$\frac{H_2O}{H_2}$	P_{O_2} (Torr)
1200	0.547	3.63×10^{-14}
1300	0.628	2.26×10^{-12}
1400	0.683	7.24×10^{-11}

APPENDIX II

CONVERSION FACTORS FOR WEIGHT GAIN TO PENETRATION DATA

CONVERSION OF WEIGHT GAIN BY OXIDATION TO METAL PENETRATION

Assuming uniform oxidation with no alloy depletion nor internal oxidation, the following relations between metal penetration and weight gain should be valid.

$$\frac{\Delta M}{A} = \Delta \chi \frac{M_o}{M_{meo}} \rho_{me} ,$$

where,

$\frac{\Delta M}{A}$ = weight gain in mg/cm^2

$\Delta \chi$ = metal penetration in cm

M_o = molecular weight of oxygen molecule

M_{meo} = average molecular weight of the metal oxide/gram molecular weight of oxygen

ρ_{me} = density of the metal, mg/cm^3.

Alloy data sheets list the metal density for Hastelloy X-280 as 8.24 g/cm^3; for Haynes Alloy 25, 9.14 g/cm^3; and for Inconel 600, 8.5 g/cm^3. The approximate metal combining weights are 95.71 g/g mole O_2 for Hastelloy X-280, 110.62 g/g mole O_2 for Haynes Alloy 25 and 86.41 g/g mole O_2 for Inconel 600.

Using these values, the factors between weight gain and metal penetration are

$$\Delta \chi (cm) = \frac{\Delta M}{A} \times \frac{95.71}{32.00} \times \frac{10^{-3}}{8.24} = 3.63 \times 10^{-4} \frac{\Delta M}{A} , \qquad (1)$$

or

$$\Delta \chi (mils) = \frac{3.63 \times 10^{-4}}{2.54 \times 10^{-3}} \times \frac{\Delta M}{A} = 0.14 \frac{\Delta M}{A} \text{ for Hastelloy X-280;}$$

$$\Delta\chi(\text{cm}) = \frac{\Delta M}{A} \times \frac{110.62}{32.00} \times \frac{10^{-3}}{9.14} = 3.78 \times 10^{-4} \frac{\Delta M}{A}, \quad (2)$$

or

$$\Delta\chi(\text{mils}) = \frac{3.78 \times 10^{-4}}{2.54 \times 10^{-3}} \times \frac{\Delta M}{A} = 0.15 \frac{\Delta M}{A} \text{ for Haynes Alloy 25; and}$$

$$\Delta\chi(\text{cm}) = \frac{\Delta M}{A} \times \frac{86.41}{32.00} \times \frac{10^{-3}}{8.5} = 3.18 \times 10^{-4} \frac{\Delta M}{A}, \quad (3)$$

or

$$\Delta\chi(\text{mils}) = \frac{3.18 \times 10^{-4}}{2.54 \times 10^{-3}} \times \frac{\Delta M}{A} = 0.12 \frac{\Delta M}{A} \text{ for Inconel 600.}$$

CONVERSION OF WEIGHT LOSS BY EVAPORATION TO METAL PENETRATION

To discuss metal penetration of alloys from weight loss measurements, the assumptions of uniform evaporation and of no preferential alloy depletion are made. Obviously, this is not the case when dealing with complex alloys. However, for a rough comparison, the following relates weight loss to metal penetration.

$$\frac{\Delta M}{A} = \Delta\chi \rho_{me},$$

where,

$\frac{\Delta M}{A}$ = weight loss in mg/cm^2

$\Delta\chi$ = penetration in cm

ρ_{me} = density in mg/cm^3 of the metal alloy.

The conversion factors are

$$\Delta\chi(\text{cm}) = \frac{\Delta M}{A} \times \frac{10^{-3}}{8.24} = 1.21 \times 10^{-4} \frac{\Delta M}{A}, \quad (4)$$

or

$$\Delta\chi(\text{mils}) = \frac{1.21 \times 10^{-4}}{2.54 \times 10^{-3}} \frac{\Delta M}{A} = 0.048 \frac{\Delta M}{A} \text{ for Hastelloy X-280;}$$

$$\Delta\chi(\text{cm}) = \frac{\Delta M}{A} \times \frac{10^{-3}}{9.14} = 1.09 \times 10^{-4} \frac{\Delta M}{A}, \qquad (5)$$

or

$$\Delta\chi(\text{mils}) = \frac{1.09 \times 10^{-4}}{2.54 \times 10^{-3}} \frac{\Delta M}{A} = 0.043 \frac{\Delta M}{A} \text{ for Haynes Alloy 25; and}$$

$$\Delta\chi(\text{cm}) = \frac{\Delta M}{A} \times \frac{10^{-3}}{8.5} = 1.18 \times 10^{-4} \frac{\Delta M}{A}, \qquad (6)$$

or

$$\Delta\chi(\text{mils}) = \frac{1.18 \times 10^{-4}}{2.54 \times 10^{-3}} \frac{\Delta M}{A} = 0.046 \frac{\Delta M}{A} \text{ for Inconel 600.}$$

APPENDIX III

DERIVATION OF WEIGHT GAIN EXPRESSION FOR THE CARBURIZATION OF SUPERALLOYS IN METHANE

EXPRESSION GOVERNING A SYSTEM UNDER GAS-PHASE DIFFUSION CONTROL

An expression for the weight gain of the metal samples due to the methane-metal reaction can be arrived at assuming gas-phase diffusion rate control in the furnace tube. For a tube of length (ℓ) and cross sectional area (A) separating the source of methane (bell jar) from the sample (see Figure 1), the following approach is suggested.

Defining

M_o = mass of carbon initially present in the system
= VC_o, and
M = instantaneous mass of carbon
= VC

where,

V = volume of bell jar and C_o and C are the respective initial and instantaneous concentrations of carbon,

then the weight gain by the coupon due to carbon pickup (ΔW) at any time (t) is

$$\Delta W = M_o - M \qquad (1)$$

The flux (J) in the tube is given by Fick's first law

$$J = \frac{dM}{dt}\frac{1}{A} = -D\frac{\delta c}{\delta x}$$

which for the above case can be rewritten

$$J = -\frac{dM}{dt}\frac{1}{A} = D\,\frac{C_b - C_\ell}{\ell} = D\,\frac{\left(\frac{M}{V} - 0\right)}{\ell} \qquad (2)$$

where

$\frac{dM}{dt}$ = rate of carbon transport

D = diffusivity of methane in hydrogen

C_b = instantaneous concentration of carbon at $\chi = 0$ (at bell jar).

C_ℓ = concentration of carbon at $\chi = \ell$. This valve represents the concentration of carbon in the gas phase near the sample, and is assumed equal to zero.

Then

$$-\frac{dM}{dt} = \frac{DA}{\ell}\ \frac{M}{v} = kM, \tag{3}$$

where

$$k = \frac{DA}{\ell v}.$$

Separating the variables and integrating

$$\int \frac{dM}{M} = \int -k\,dt \tag{4}$$

$$\ln M = -kt + B \tag{5}$$

where

B = integration constant.

Using Equation (1), (5) becomes

$$\ln(M_o - \Delta W) = -kt + B, \tag{6}$$

or

$$M_o - \Delta W = e^{-kt}e^{B} = B' e^{-kt},$$

or

$$\frac{M_o - \Delta W}{B'} = e^{-kt}.$$

But at $t = 0$, $\Delta W = 0$: thus, $M_o = B'$.

Then

$$\frac{M_o - \Delta W}{M_o} = e^{-kt} = e^{\frac{DA}{\ell v}t}, \tag{7}$$

or

$$\ln\left(1 - \frac{\Delta W}{M_o}\right) = -kt = -\frac{DA}{\ell v}t.$$

REFERENCES

1. L. S. Darken and R. W. Gurry. Physical Chemistry of Metals, McGraw-Hill Book Company, Inc., New York, 1953. p. 349.

2. F. C. Rosenthal. Unpublished Data. General Electric Co., Richland, Washington. July 24, 1963. (Personal Communication)

3. F. C. Rosenthal. Unpublished Data. General Electric Co., Richland, Washington. July 24, 1963. (Personal Communication)

4. R. L. Knecht. Dissimilar Metal Welds of Certain Superalloys and Stainless Steels, HW-78574. August, 1963.

5. R. Simenz. "This Test for Oxidation Resistance," Product Engineering, vol. 30, pp. 48-50. 1959.

6. S. T. Wlodek. "The Oxidation of Hastelloy Alloy X," Transactions of the Metallurgical Society of AIME, vol. 230, pp. 177-185. 1964.

7. S. T. Wlodek. "The Oxidation of Rene' 41 and Udiment 700," Transactions of the Metallurgical Society of AIME, vol. 230, pp. 1078-1090. 1964.

8. O. Kubaschewski and B. E. Hopkins. Oxidation of Metals and Alloys, Butterworths, London. 2nd ed., pp. 130-142. 1962.

9. D. Caplan and M. Cohen, "The Volatilization of Chromium Oxide," J. Electrochem. Soc., vol. 108, pp. 438-441. 1961.

10. R. C. Bates. "Evaporation Rates of Several Alloys in Vacuum at High Temperatures," Metal Treating, vol. 12, pp. 16-18. 1961.

11. J. S. Brunhouse. Unpublished Data. Aerojet General Nucleonics, San Ramon, California. (Personal Communication)

12. Quarterly Progress Report, Metallurgy Research Operation, July, August, September, 1964, edited by J. J. Cadwell, HW-84281. General Electric Company, Richland, Washington. October 15, 1964.

13. Quarterly Progress Report, Metallurgy Research Operation, October, November, December, 1964, edited by J. J. Cadwell, HW-84573. General Electric Company, Richland, Washington. January 15, 1965.

REFERENCES (Contd.)

14. K. Osthagen. "Oxidation of 80 Ni-20 Cr Alloy in Carbon Monoxide at High Temperatures," Corrosion, vol. 20, pp. 438-441. 1961.

15. S. Dushman and J. M. Lafferty, eds. Scientific Foundation of Vacuum Technique, John Wiley and Sons, Inc., New York, p. 773. 1962.

16. R. E. Woodley. Unpublished Data. General Electric Co., Richland, Washington. May, 1962. (Personal Communications)

17. S. Dushman and J. M. Lafferty, eds. Scientific Foundation of Vacuum Technique, John Wiley & Sons, Inc., New York, pp. 753, 755, 757. 1962.

ONSITE DISTRIBUTION

Copy Number

Pacific Northwest Laboratory

1	F. W. Albaugh
2	J. A. Ayres
3	A. L. Bement
4	T. K. Bierlein
5	S. H. Bush
6	J. J. Cadwell
7	L. A. Charlot
8	T. T. Claudson
9	L. J. Defferding
10	D. R. deHalas
11	R. L. Dillon
12	A. B. Johnson
13	D. C. Kaulitz
14	G. A. Last
15	J. E. Minor
16	R. E. Nightingale
17	D. P. O'Keefe
18	W. E. Roake
19	D. W. Shannon
20	V. H. Troutner
21	R. E. Westerman
22	R. G. Wheeler
23	O. J. Wick
24	F. W. Woodfield
25	300 Technical Publications
26	700 Technical Publications
27 - 31	Technical Information Files
32 - 62	Extra

General Electric Company, Richland

63	D. H. Curtiss
64	M. Lewis
65	GETA File Copy

Richland Operations Office

66	R. K. Sharp
67	Technical Information Library